Mastergradsoppg. 2011

Strain measurements on glulam beams with holes

Gunhild Medhaug

Norwegian University of Life Sciences
Department of Mathematical Sciences and Technology
Master Thesis 30 credits 2011

Contents

The Norwegian University of Life Sciences and Technology
Department of Mathematical Sciences and Technology

1. Intoduction

1.1. The mechanical challenge

In structural design it is sometimes necessary to make holes through glulam beams. A hole in a glulam beam subjected to bending, reduces the strength significantly due to the development of stress concentrations establishing high perpendicular to grain tensile stresses and shear stresses in the vicinity of the hole (Aicher and Höfflin 2008), see figure 1.

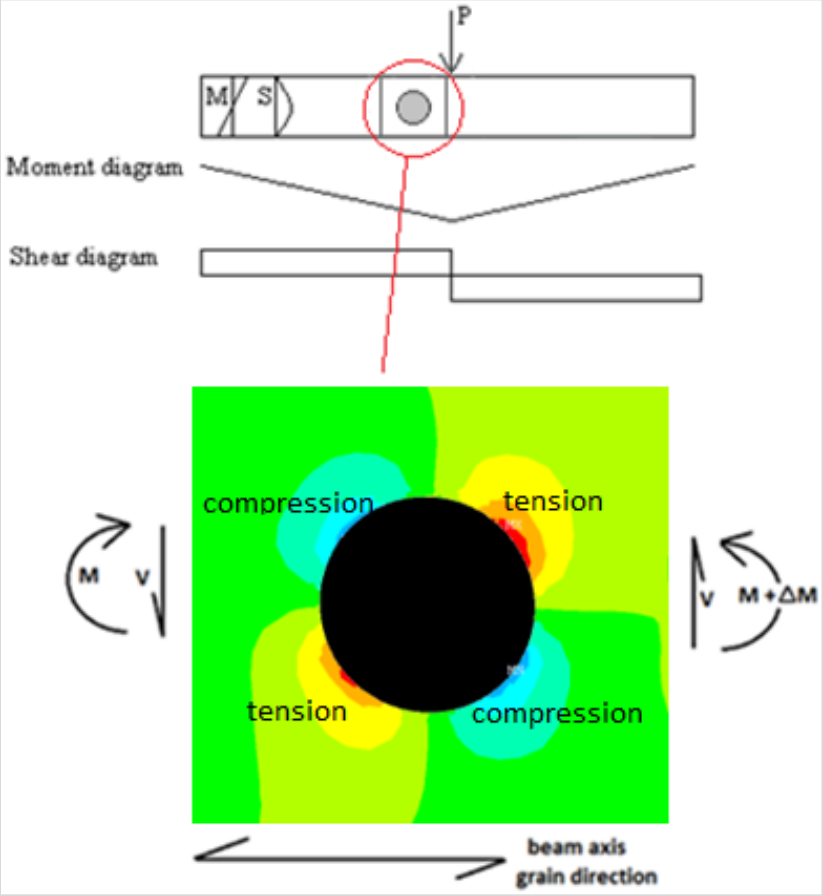

Figure 1: Stress distribution perpendicular to grain (Aicher and Höfflin 2008)

The Norwegian University of Life Sciences and Technology
Department of Mathematical Sciences and Technology

Wood is anisotropic i.e. its mechanical properties are direction dependant. The strong structure of wood is predominantly in the longitudinal direction of the grain. This is especially manifested in tension as the tensile strength across the fibers is 3 - 5 % of the tensile strength along the fibers (Kollman and Cote 1968; Bodig and Jayne 1982). The resistance to crack propagation ensues from the strength properties in wood, and is consequently critically low perpendicular to the fiber direction when exposed to transversal tension(Gustafsson 2003), see Figure 2 and Figure 3. Fracture caused by tension perpendicular to grain commonly has a brittle course.

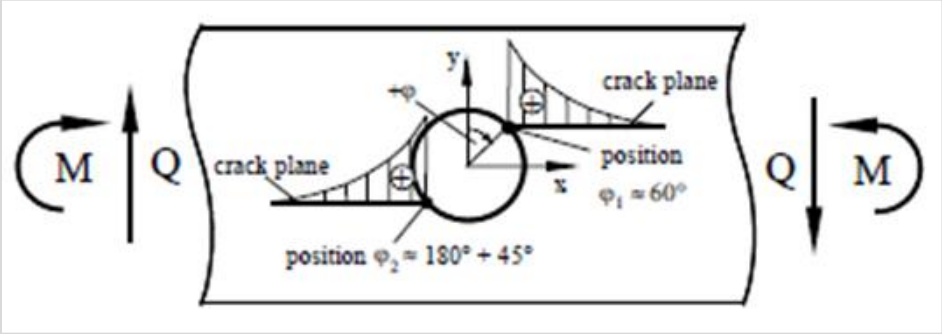

Figure 2: Schematic illustrations of distribution of tension stresses perpendicular to grain along (Aicher and Höfflin 2004)

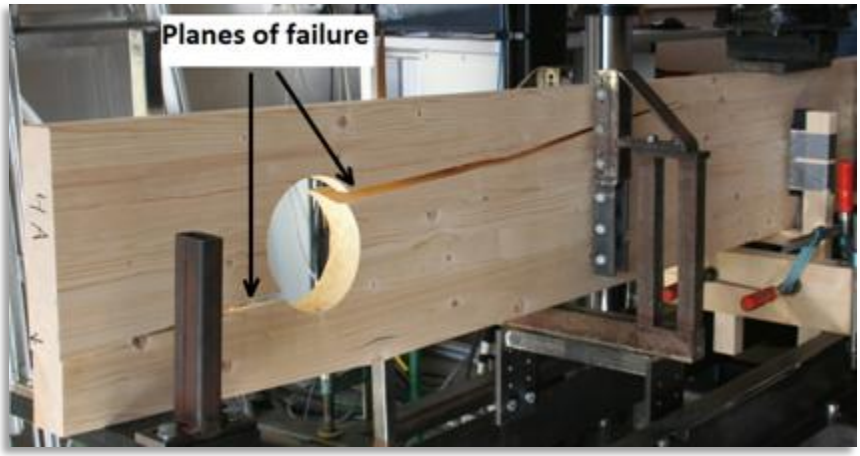

Figure 3: Glulam beam with hole subject to bending

The Norwegian University of Life Sciences and Technology
Department of Mathematical Sciences and Technology

1.2. Earlier work

The analysis of holes in glulam beams has been subjected to a number of discussions and research the past four decades. Henrik Danielsson (2009) did an extensive compilation study of experimental and analytical research that had been performed on the area. A short summary of the works Danielsson included follows below.

Kolb and Frech (1977) used Bernoulli-Euler beam theory to analyze the maximum normal stress due to bending, and the maximum shear stress in glulam beams with holes. An empirical expression was derived in order to predict the strength capacity of the beam. The expression was based on a reduction of the shear force capacity with a factor determined by the ratio of the beam height and the reduced height due to the hole. The capacity of the beam was heavily underestimated compared to test results.

Penttala (1980) analytically determined the state of stresses with plate theory and functions proposed by Kolosov and Muskhelishvili, using both isotropic and anisotropic material models. The stress at the edge of the hole was compared to the material tensile strength determined by Hankinson's formula.

Johannesson (1977; 1983) used three different stress based methods to analyze the strength of the tested beams ("Shear-stress", "Navier-beam" – and "Exact-stress" method). A linear elastic material model was used for all analyses.

The "Shear – stress" method is an empirically based method comparing shear strength with a fictive shear strength determined from experimental tests.
The "Navier-beam" method was developed to enable hand calculation more reliable than the "Shear-stress" method. The maximum hoop stress in the cross section of the hole boundary is calculated and compared to a corresponding strength value determined from material tests.

The “Exact-stress” method calculates the stress distribution by three different methods: closed form analytical solution, the finite element method and the boundary-element method. In addition to assuming a linear elastic material model, plane state of stress and thus a two dimensional orthotropic model was assumed, ignoring the influence of the cylindrical shape of the annual rings. A simplified version of the Norris failure criterion [1] (Norris 1962) was used in connection with this method, considering only the perpendicular to grain stress and strength:

$$\left(\frac{\sigma_2}{f_2}\right)^2 = 1 \qquad [1]$$

Riipola (1995) did an analytical study using a fracture mechanic approach. Expressions for strain energy release rate for two different loading mode types of fracture were derived, and the stress intensity factor was determined from these expressions. The load bearing capacities were further evaluated by comparing the stress intensity factors and experimentally determined critical stress intensity factors. The method is valid for holes placed in a shear force dominated area. An extra correction factor was used for holes placed close to support.

Scheer and Haase (2000[1])determined stress concentrations near elliptical holes in glulam beams using analytical formulations according to Lekhnitskii and Savin. A Finite Element Method model was used in order to verify the analytical solutions. For the analytical calculations, the beam was modeled as a plate with a plane state of stress and orthotropic material properties. In part two of their report (2000[2]) Scheer and Haase used a fracture mechanic approach determining stress intensity factors at fictitious cracks with the finite element method and the Rice integral. The beam was modeled in two dimensions as an orthotropic material.

Stefansson (2001) performed strength analyses on timber beams with holes using Linear Elastic Fracture Mechanics (LEFM) and Non Linear Fracture Mechanics (NLFM) in Finite Element analyses. A crack was modeled in a critical region and strength analysis of the beam was performed for various lengths of the crack using the energy release rate approach. A plane state of stress was assumed and a linear elastic

and orthotropic material model was used. The NLFM analyses are based on the fictitious crack model and applied by means of interface elements with a piecewise linear stress-deformation relationship on a prescribed crack path.

Höfflin's doctoral thesis (2005) deals with the capacity of glulam beams with holes and includes extensive experimental testing on different beam and hole geometries. The state of stresses in the vicinity of the hole was further examined by means of finite element analysis. Both 2D and 3D finite element analyses were carried out. The distribution of normal and shear stresses along the hole perimeter was investigated and maximum tensile stress perpendicular to grain was located. The two dimensional analysis were performed assuming plane state of stress and an orthotropic material model. The three dimensional model considered the variation of stress perpendicular to grain across the beam width in the vicinity of the hole.

Höfflin proposed a method for design of glulam beams with holes based on Weibull weakest link theory. The heterogeneity and the stress distribution in the material are considered by a form factor indicating the ratio between the maximum stress at an uneven stress distribution and the equivalent Weibull stress corresponding to the same probability of failure. The calculations are to a great extent dependent on the stressed area chosen for integration.

Aicher and Höfflin (2008) reported experimental investigations on glulam beams with holes, representing a consistent data base for the specific structural problem. The two major aspects of size effect[1] and specific damage evolution[2] were quantified. The Weibull theory based model (Höfflin 2005) was further developed and calibrated to the shear force capacities at ultimate load and to the loads associated with a crack over full width at the hole wall prior to ultimate load. The bending moment to shear force ratio is considered in the proposed model by a section force combination factor.

According to Gustafsson and Enquist (1988), a drawback of the Weibull theory is that it cannot be applied to strength analysis of structural elements with a stress singularity caused by a crack or a sharp notch.

[1]: Size effect: there is not a linear relation between increased cross section of the beam and increased load carrying ability as larger volume of wood implies a larger scatter of material properties.

[2]: The specific damage evolution: The stages of crack propagation were also defined and quantified.

Danielsson and Gustafsson (2010) proposed a new design model for glulam beams with holes. The model, the Probabilistic Fracture Mechanic method (PFM), is based on a combination of Weibull weakest link theory and a mean stress method which is a generalization of linear elastic fracture mechanics. Considering decisive material properties like material strength, the fracture energy and the heterogeneity, the PFM model shows good ability to predict the strength of glulam beams with holes with exception of small beams (H = 180mm).

There has been a significant progress in the knowledge of strength capacity and the affecting cause of weakening the strength capacity of glulam beams with holes, resulting in better design model proposals.

1.3. Motivation

The starting point of this study was the situation for Norwegian engineers lacking trustworthy design rules for glulam beams with holes. The Norwegian design code for timber (NS 1999), provide design recommendations based on Johanneson's "Shear-stress" method described above. The "Shear-stress" method is an ultimate limit state shear control of the residual cross-section of the beam. Bending moment effects are not considered. The geometry criteria in themselves are so conservative that the practical accomplishment of introducing a hole in a glulam beam is difficult. Further, the contemporary version of the European timber code Eurocode 5 (1995-1-1 2004) contains no design recommendations for beams with holes.
Even though there have been significant improvements in modeling the load carrying capacities the last years, there is still indication of the need for more research and experimental verification.

In earlier research, the stress concentrations in the vicinity of the hole have been modeled, and load carrying predictions have been estimated by proposed design models. The actual stress values are however calculated by means of Finite Element Models and material properties are found from other sources.

1.4. Aim and Scope

The aim of this study is to substantiate attained knowledge of stress concentrations appearing in the vicinity of a hole in a glulam beam subject to bending by measuring the different strains (ε_x, ε_y and ε_{xy}) that occur on the surface of experimentally tested beams in a limited area around the hole.

It is decided to focus on one specific parameter, the influence of bending moment on the strain concentrations in the vicinity of the hole, and thus the influence of bending moment on the load bearing capacity of the beam.

Bending moment gives rise to compressive and tensile normal stresses governing the upper and the lower part of the beam respectively. The hole will cause these stresses to act at an angle to the grain, thus there is a perpendicular to grain stress component and a longitudinal stress component (Johannesson 1983). In addition, the compressive normal stresses will result in passive tensile stresses appearing perpendicular to grain. Aicher and Höfflin interpreted this consequence of compression in the upper part of the beam differently in “A contribution to the analysis of glulam beams with round holes” (2000): “Functionally seen, the tension stresses [perpendicular to grain] act as “hold back” stresses for the inclined bending compression stresses”.

Experimental results from tests performed by Höfflin and Aicher (2005; 2006) showed a significant strength decreasing effect of high ratio of section forces, i.e. bending moment to shear force ratio, in the vicinity of the hole.

"The location and the magnitude of the peak stress of the whole tension perpendicular to grain stress field depends essentially on the loading condition of the beam, i.e. on the ratio of bending moment, M, to shear force, V, at the hole location." – (Aicher and Höfflin 2004)

Danielsson and Gustafsson (2010) evaluated the proposed model (PFM) against experimental results with respect to, among other parameters, bending moment to shear force ratio. It was found that for holes centrically placed with respect to beam height, PFM predicts decreasing strength for increasing bending moment to shear force ratio, though the differences in strength are comparatively small.

It is out of the scope of this study to evaluate the load bearing capacity with respect to bending moment to shear force ratio on the tested beams against the corresponding ratio predicted by PFM.

In this study, there will be performed experimental tests of paired split beams with different hole position along the longitudinal axis, varying the size of bending moment.

The load reaction of the test beams will be accurately determined by measuring strains of a limited area in the vicinity of the hole of the glulam beams by means of photogrammetry. Photogrammetry has shown advantageous in the field of deformation measurements on small specimen as it allows precision analysis of an object without physical contact with it (Choi, Thorpe et al. 1991; Franke, Franke et al. 2007; Dahl 2009). Any mechanical influence from the testing equipment on the test beams is thus avoided. The capability of measuring large deformations, even beyond component failure is highly beneficial, and will be performed in this study.

A secondary aim of this study is to perform linear and non-linear Finite Element Method (FEM) analyses of the tested beams and evaluate the analytical results against the strains derived from the photogrammetric results.

For the clarity of geometry, it will be referred to Figure 4.

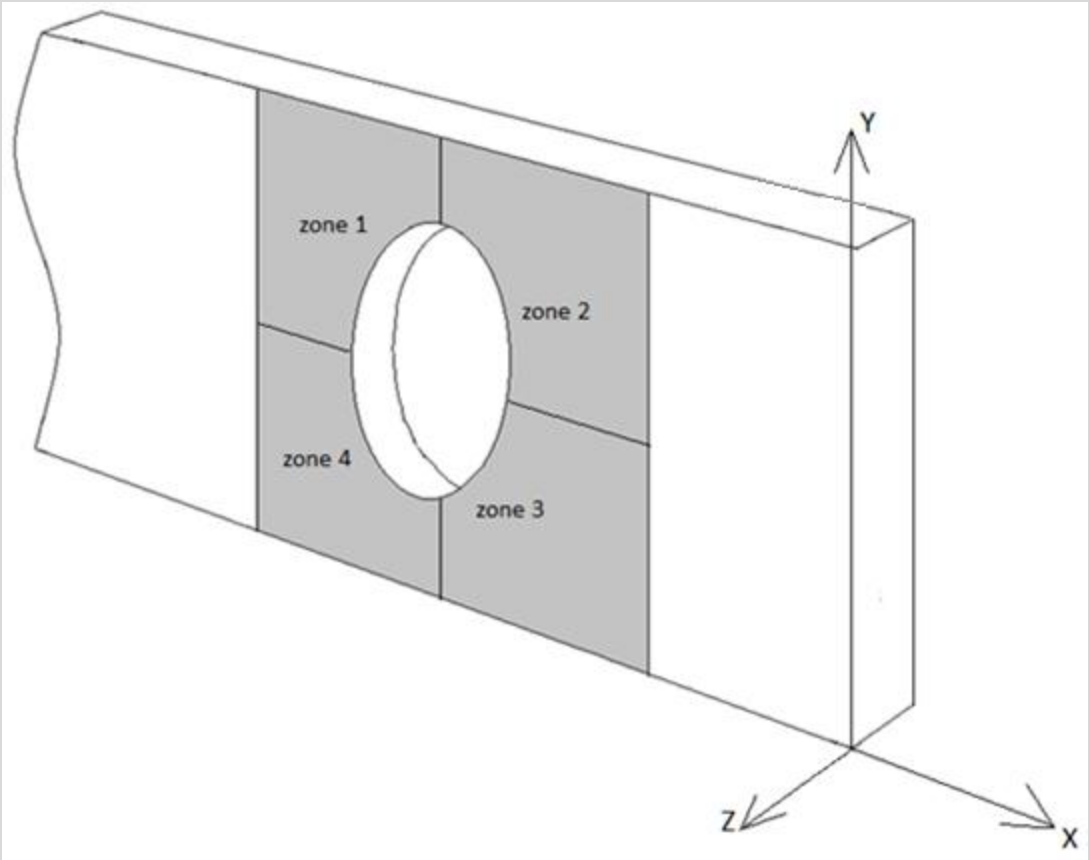

Figure 4: The geometry denotations of the tested beams

2. Material and method

2.1. Experimental procedure

2.1.1. Test set-up

Experimental tests of glulam beams with holes were carried out. The randomly chosen glulam beams were built of 7 lamellas of Norway spruce of quality L40. Ten glulam beams were loaded with a three point load until failure (Figure 1). The tested beams were originally five 115 x 315 mm glulam beams. Each of these beams was split in two and holes were introduced on different positions along the longitudinal axis. One of the paired beams had a hole close to support (beam type A), and the other beam had hole close to the load (beam type B). Figure 5 specifies the dimensions for the position of the holes, and the beam geometry.

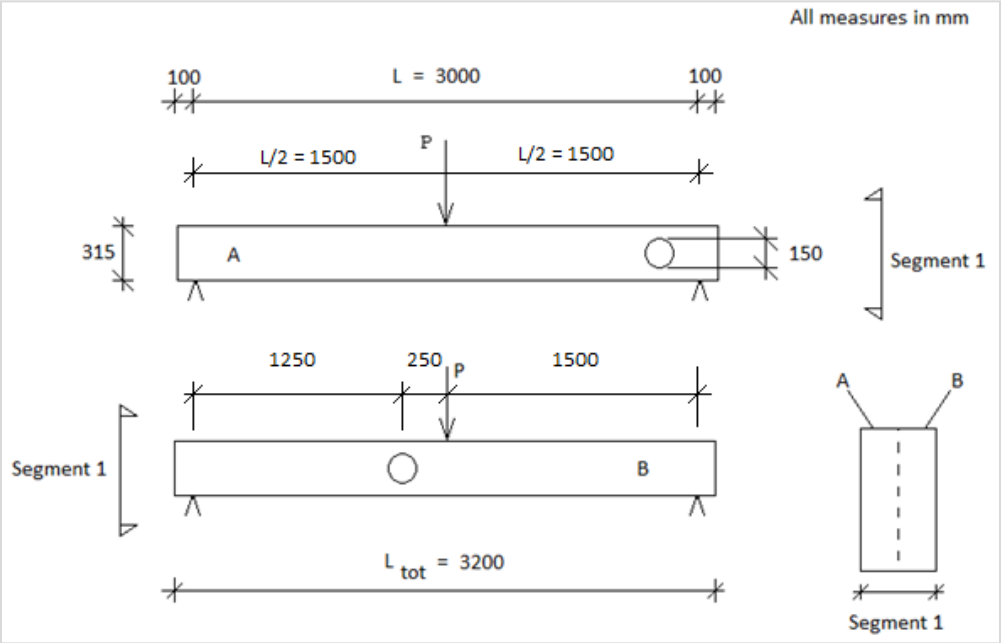

Figure 5: The test set-up

The beams were fixed in a universal loading frame and were prohibited from moving sideways by two u brackets. The u brackets had vertical rollers to prevent coercive forces. The load was positioned at the middle of the beam with a constant speed of 1 mm per second until failure. A 300 kN hydraulic, universal and static UTM testing machine from Instron (KN300J5844), was used to perform the tests. The loading time per beam was approximately between 10 and 15 minutes.

A total number of 312 equally sized circular dots were applied to the wood surface with a black ballpoint pen in a quadratic 20 x 20 grid system. The vertical and horizontal distance between the dots was 15 mm.

Measurements were done on the longitudinal radial plane, see Figure 6

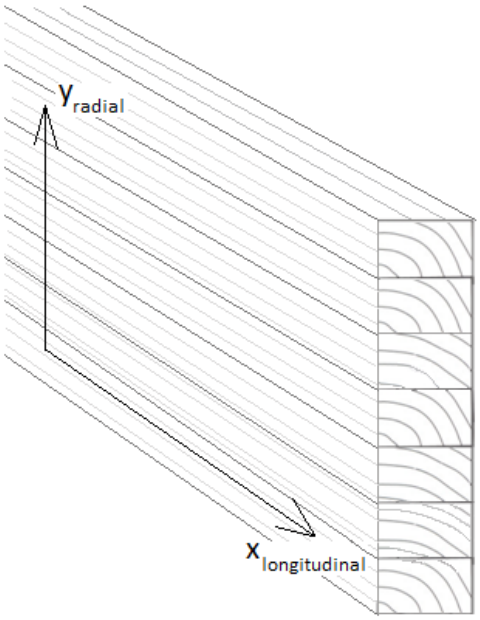

Figure 6: The grid that was measured was on the surface of splitting, i.e. in the longitudinal radial plane

2.1.2. Practical photogrammetry

Two cameras were mounted on a rigid tripod 800mm away from the hole in the beam, see Figure 7 and 8. It was decided to use two cameras in order to gain any possible three dimensional information from the measuring grid, and also to sample data from two independent sources with the purpose of finding the mean of the two sets of data as this would be statistically preferable. The two cameras were positioned with a small horizontal angle during testing, confer Figure 8. The camera on the left hand side did not keep a continuous frequency during testing, which led to the conclusion of only analyzing data from the right hand side camera. The angle of the camera that was used to collect data caused inaccurate measurements as the scale changes from the left to the right in the picture. This inaccuracy is the same for both beam types. A correction was therefore not necessary as the focus in this study is comparing strains in beam type A and beam type B.

Figure 7: Testing of beam 3B

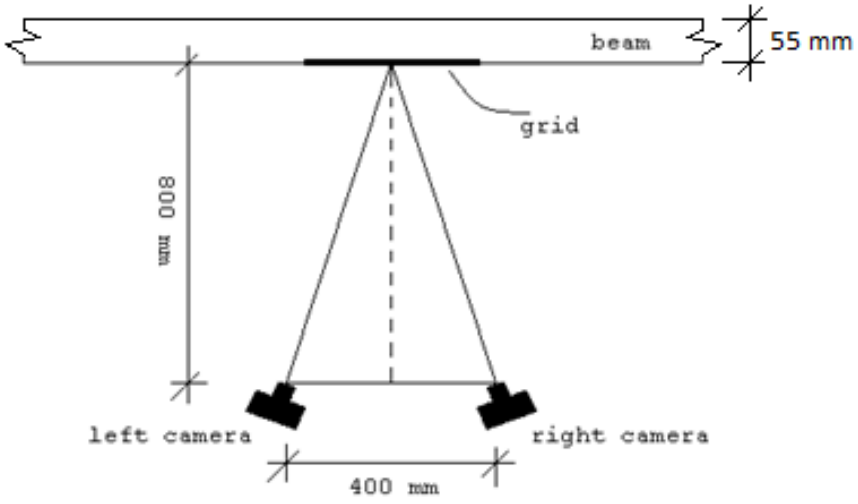

Figure 8: Camera position

Adequate contrast between the dots and the beam surface are decisive for the result of the measurement as the algorithm used to detect the dots from the pictures, evaluates the grey contrast transition between the surface and the dots. Applying the dots directly on the beam surface without any pretreatment of the wood proved disadvantageous due to knots and other irregularities in the lumber, complicating the process of detecting the dots. Treating the measuring area with a white wax glaze before applying dots is therefore recommendable.

The measuring field was illuminated by a source of fluorescent light. In the post processing of detecting the dots on the wood surface, it was discovered that a better light source would be desirable as the single fluorescent light source used did not provide sufficient illumination of the measuring area. Further, disturbance from sunlight and movement in the room made it difficult to automate the algorithm for detecting dots, as the grey contrast transition between the wood surface and the marked

dots is affected from the uneven lighting. More manual work was thus required in order to interpret the data from the pictures.

Due to the massive manual work required to interpret the data from the pictures, only six of the originally ten beams were analyzed.

The measuring grid will deform locally as the load increases, and as the beam is gradually bended, the grid will follow the global deformation as well. Having a fixed point independent of the beam is therefore imperative in order to find correct dot coordinate values. Origin, defined at a point to the left of the grid, is continually regulated in relation to the fixed point. Dots marked on a steel frame, clamped to the loading frame, were used as reference points see Figure 9. The reference points also functioned as safety against any sudden camera movements.

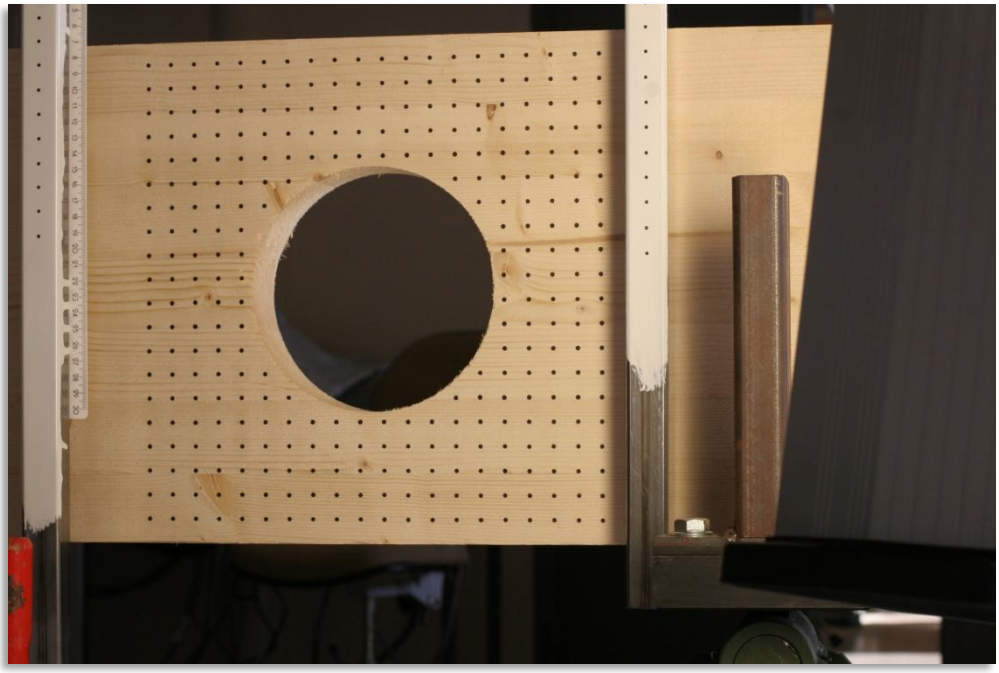

Figure 9: Steel frame securing fixed reference points

2.1.3. Density measurement

After the experimental tests were carried out, small tests were taken from every lamella in every beam. Weight and moisture content was measured and basic density was calculated. The basic density for the evaluated test beams are presented in Table 3.

2.2. Experimental apparatus

The data acquisition was performed by means of a single-lens reflex camera of type Canon Eos 20D, with 8,2 MP resolution and a 22,5x15 mm CMOS sensor. A 50 mm objective was used ensuring close to correctly reproduced angles and measures across the field view. The aperture was 5,65564, exposure time was 1/125, and the ISO was set to 400.

Marked dots on the beam surface area surrounding the hole were photographed every second of the test duration. The in plane coordinates x and y of the dots were thus registered the entire loading period until failure. Every dot corresponds to approximately 19 pixels, which provides high certainty of measurement and secures observation of every movement in the grid.

2.3. Post processing of data

2.3.1. Photogrammetry

The image file format information was adjusted to correlate with the time and log files from the experiment. Every picture was then analyzed in Scorpion (Tordivel), software specialized in making 2D and 3D machine vision systems. The pictures were subsequently calibrated and the dots were localized by means of an algorithm called “Blob finder 3”. The center of mass for every dot was calculated and the corresponding coordinate values were found.

2.3.2 Strain calculations of experimental results

An algorithm was developed in order to designate strains from the coordinate values. Similar to the FE model, the algorithm calculate the strain of each node. In order to smooth the deformation data the photogrammetric analysis provided, vertical and horizontal strains were calculated from deformation of length between three nodes. The shear strains were found by calculating the mean change of angle $\alpha + \beta$, refer Figure 10. The calculations were based on the deformation of x and y- length and angle of an axe- system covering 9 nodes. The deformation was assigned as a property of the origin, i.e. the center node. Every node represented the center of an axe- system, thus we got 312 axe- systems in the grid. The progression of deformation in the vicinity of the hole is described in detail by the information subscribed to every node by the appurtenant axe - system.

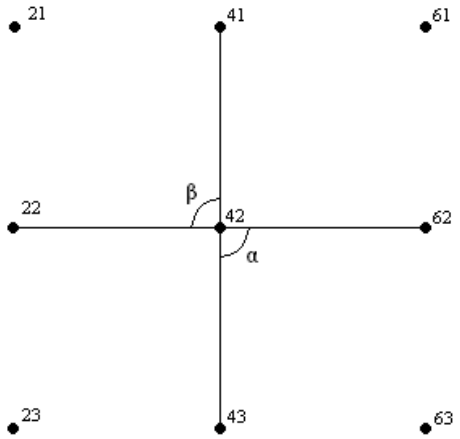

Figure 10: The axe system used in calculating strains from experimental results

The strain calculations for the nodes placed on the grid edges has half the accuracy as neighboring nodes lack on one side.

During the experiment, the load was registered for every picture, i.e. every second of the loading time. For the purpose of smoothing the experimental results, the average load and displacement of each 20 seconds period were calculated and used in the following calculations. Every beam had between 20 – 40 load steps, where each load step represented the mean load of 20 seconds.

2.4. Numerical models of experiments

In order to study the behavior of glued laminated wood in the vicinity of a hole from a numeric and analytical point of view, a Finite Element Method (FEM) approach was chosen by use of ANSYS 13.0 (ANSYS[1]).

For softwood species with relatively few amounts of ray cells compared to species like oak and beech, there are small differences between the material properties in the tangential and radial direction (Kollman and Cote 1968). As the tested beams were of Norwegian spruce, it was assumed a transverse isotropic material behavior in the numeric analysis performed in this study. The tangential/radial component was assumed equal trough the cross section of the beam. This allows for a 2D- projection to explain the 3D volume of a simplified beam structure, thus reducing the number of required elements significantly.

The two dimensional PLANE42 element (ANSYS[2]) was used to build the model in ANSYS, see Figure 11. This element is geometrically defined by four nodes having two degrees of freedom at each. A detailed description of the element type can be found in (ANSYS[2])

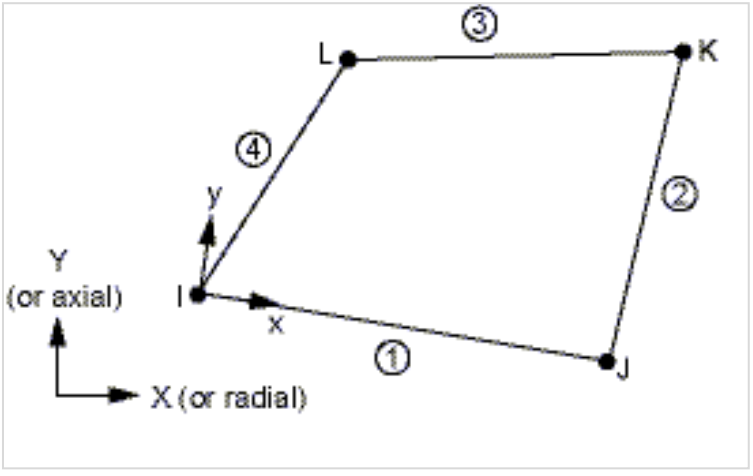

Figure 21: The PLANE42 element used in the numerical analyses *(ANSYS[2])*

The distance between the nodes in the vicinity of the hole was 15mm, securing a grid of nodes similar to the one on the test beams.

The analysis was run by constant load input, and was therefore run for every load step corresponding to every beam of type A and B

Beam A and beam B were modeled with geometry given in figure 1, and with mean value material parameters found in a recent study from Dahl (2009) given in Table 1.

Table 1: The material parameters governing the material properties of the model

	ρ (kg/m^3)	G (N/mm^2)	E_x(N/mm^2)	E_y(N/mm^2)	υ_x	υ_y
Dahl	420	611,5	9355	585	0,0775	0,598

The possibility of modeling non linear tension effects was explored to some degree. This was done using a method called “killing of nodes (KON)”. When the stress level in a node exceeds a certain level, the node loses its connecting. The level was determined based on the commonly known Norris equation [2] (Norris 1962)

$$F_N = \sqrt{\left(\frac{\sigma_x}{f_{t0}}\right)^2 + \left(\frac{\tau_{xy}}{f_{vk}}\right)^2} \qquad [2]$$

The material strength input is an estimated mean value based on the glulam quality that was used in the experimental results, and is given in Table 2.

Table 2: The material strength input values used in the numerical analysis

	f_{t0} (N/mm^2)	f_{vk} (N/mm^2)
Mean values	0,7	4,6

Tension forces perpendicular to grain in addition to shear force are the governing factors in opening and propagation of cracks in the vicinity of a hole (Danielsson and Gustafsson 2010). In order to control the propagation of cracks in the model, the component that considers longitudinal stress in the Norris criterion was omitted. Test simulations were run with the full Norris criterion, and the longitudinal tensile stress values exceeded the strength in several nodes in the lower part of the beam. As wood has an ability to handle high local longitudinal tension, including the longitudinal component could disturb the brittle behavior resulting from transversal tension and shear. Erroneous load reactions in the grid would affect the entire grid, it was therefore desirable to limit KON to the critical load reactions that in reality give rise to crack opening.

Compression forces perpendicular to grain was not treated with KON.

KON was limited to the nodes in the nodal measurement grid in vicinity of the hole. This was done to reduce singularity problems and other stress concentration related problems in transition between steel and wood and sharp corners. Global deformations could therefore be slightly influenced, but only at a non-significant level as we focus mainly on relative deformation between nodes in the vicinity of the hole.

The model is in itself linear, but it was added a non linearity to it when KON was activated. Figure 12 presents the course of the analysis of one single load step. Line A denoting the relation between load and strain before KON is activated, and line B denoting the same relation with active KON decreasing the E modulus of the grid nodes. The principle of the work diagram for the full model of the beam with all the load steps is presented in Figure 13.

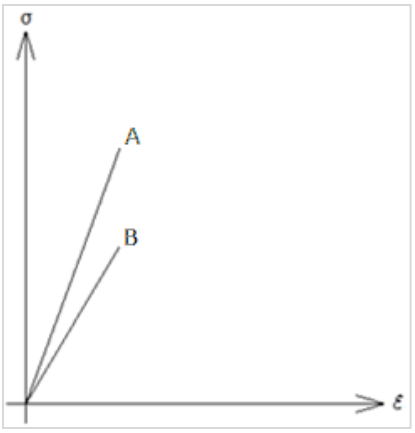

Figure 12: The work diagram for one load step

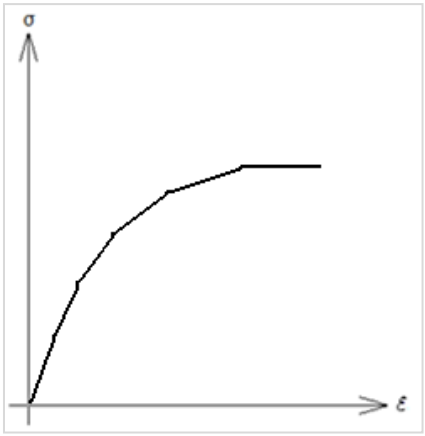

Figure 13: The work diagram for the model consisting of all load steps

2.5. Statistics

Statistical analyses were done by JMP 7.00 (SAS statistical discovery).

3. Results and Discussion

3.1. Failure loads for experimental tests

The failure load of the tested beams indicate a decreased load bearing capacity for beam type B. Ten beams are included in Figure 14. One dot denotes the relationship between failure load for each paired split glulam beam type A and type B. This provide information about the difference in failure load due to the hole position, and thus the effect of the bending moment on the bearing capacity.

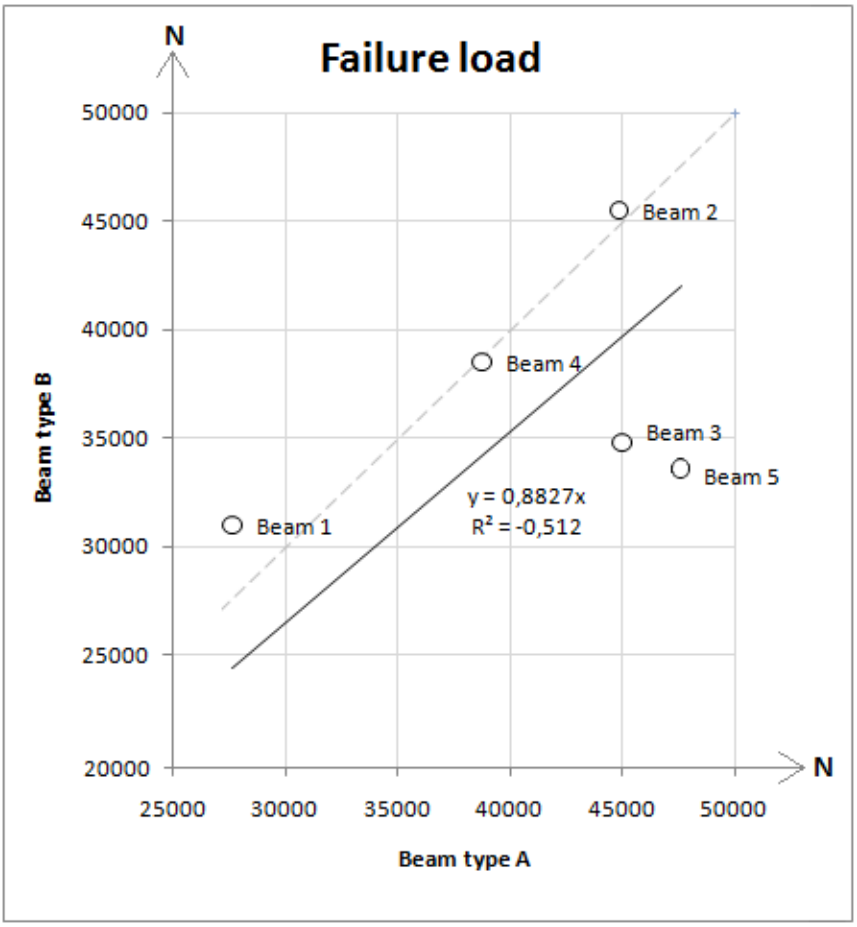

Figure 34: The failure loads of the ten tested beams

The regression line indicates lower failure load for beam type B, with a slope of -0,512. Beam 1 and beam 2 deviates from the tendency. One probable explanation is that the first four tests (1A, 1B, 2A, and 3A) had no steel plate between the load cell and the beam, resulting in considerable crushing of fibers and large local deformation. Beam 2A had, in addition to severe local deformation, a critical knot in the compression governed zone 3, refer Figure 4, see Figure 15. Still the failure load of beam 2A and 2B are similar (44808,9 N and 45522,1 N respectively), substantiating the weakening effect of bending moment on the load carrying ability to glulam beams with holes.

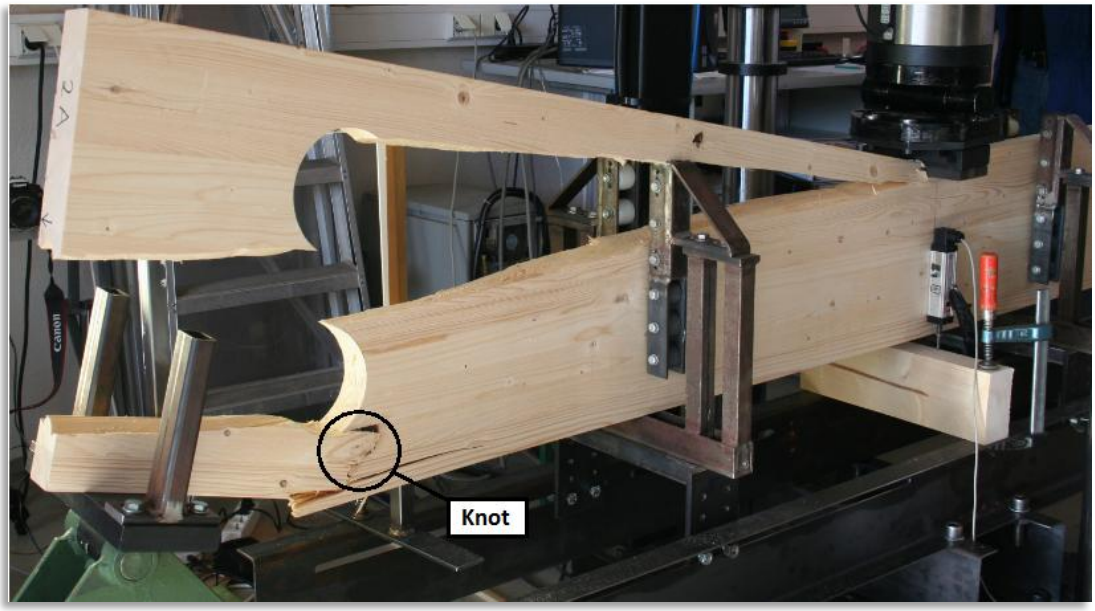

Figure 15: Fracture of beam 2A

A one sided T – test for the failure load of the ten tested beams gave no significant difference between A and B beams and bearing capacity (DF: 4, T: 1.2, P-value: 0.15). A T-test excluding the first four beams (1A, 1B, 2A and 3A) also declared non significance (DF: 1, T = 1.03, P-value: 0.25), this most probably is due to the small number of replicates.

3.2. Numerical results

Axial and shear strains were determined by 2D plane stress finite element analysis by the commercial software ANSYS (ANSYS[1]). A linear and non – linear analysis were performed for the two beam types.

In the presentation of numerical results it is focused on normal strains in the y- direction, and shear strains.

The strain results from the numerical analysis are presented below. The contour plots show the distribution of strains at a certain load level corresponding to a load towards the end of the linear elastic range for the test beams.

3.2.1. Linear analysis

3.2.1.1. Vertical strains

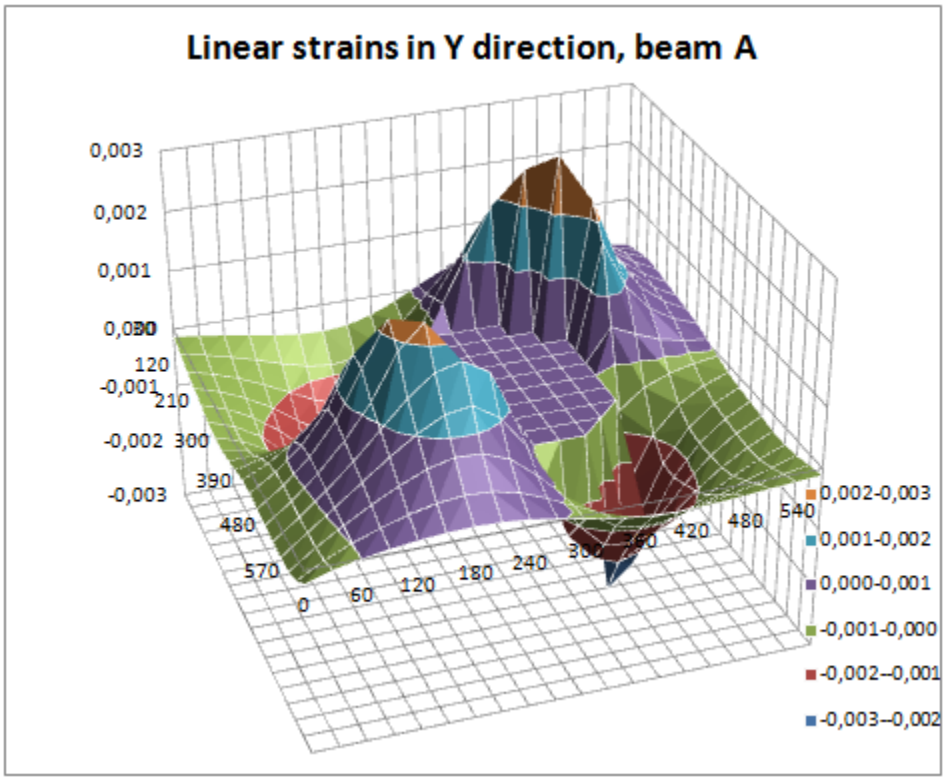

Figure 16: Normal strains in y- direction of the hole of beam A at load 28 750N

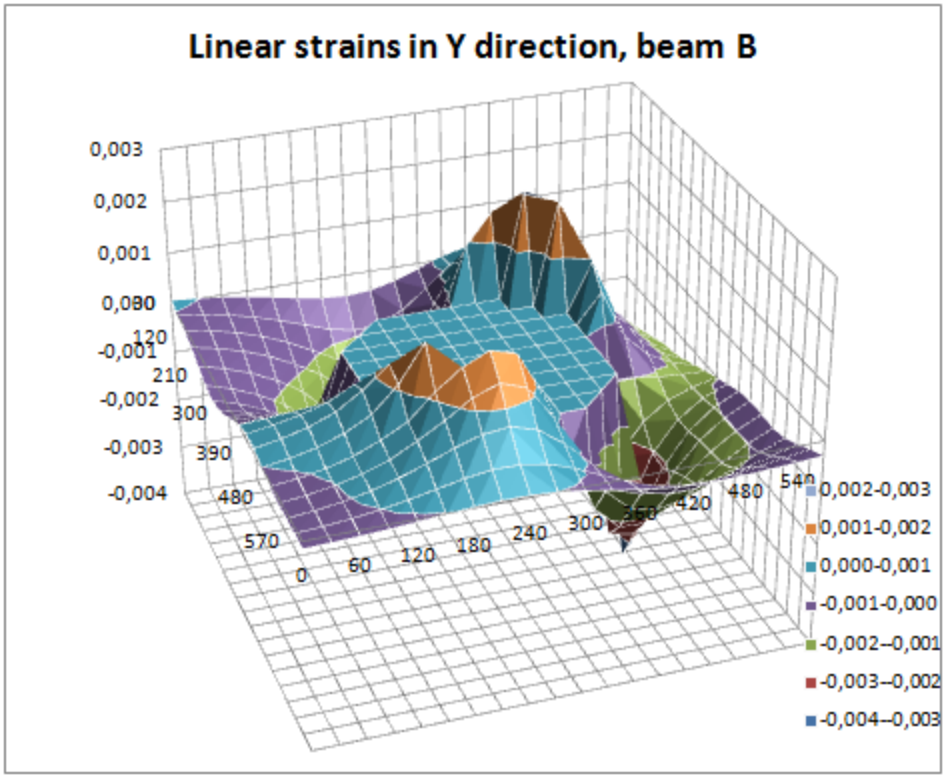

Figure 17: Normal strains in y- direction in the vicinity of the hole of beam B at load 29 190N

The output strain results shows maximum vertical tensile strains in zone 2 for both beam types refer Figure 16 and 17. The strain peak in beam A is of nearly 50 % higher value than the strain peak in beam B. A possible explanation is that the analysis emphasizes the superposed transversal compression, i.e. the local compression due to the steel plate under the load cell, counteracting the transversal tension in zone 2 for beam B. An additional explanation can be that the analysis interpret an edge fringing effect on the hole vicinity of beam A, giving less resistance from surrounding mass and thus resulting in larger strains in beam A than in beam B. Figure 17 shows that the y- directional tensile strain peak in zone 2 is closer to the upper beam edge for beam B, where the bending moment to shear force ratio is high.

3.2.1.2. Shear strains

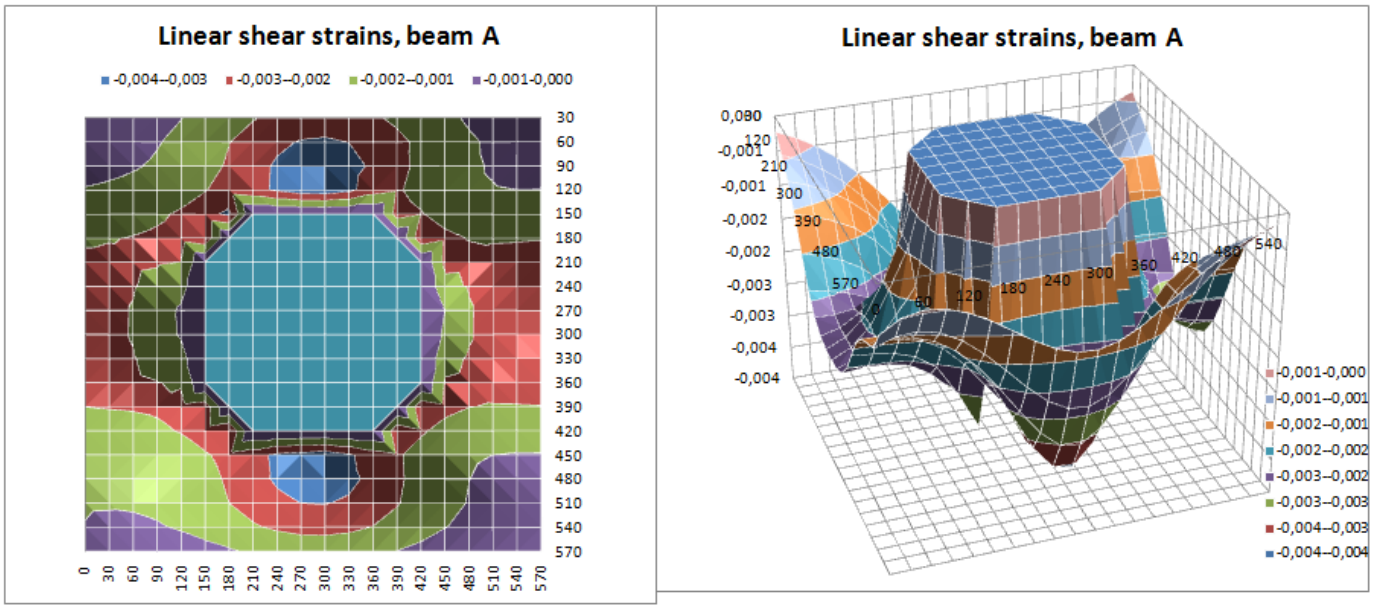

Figure 18: shear strains in the vicinity of the hole at load 28 750N

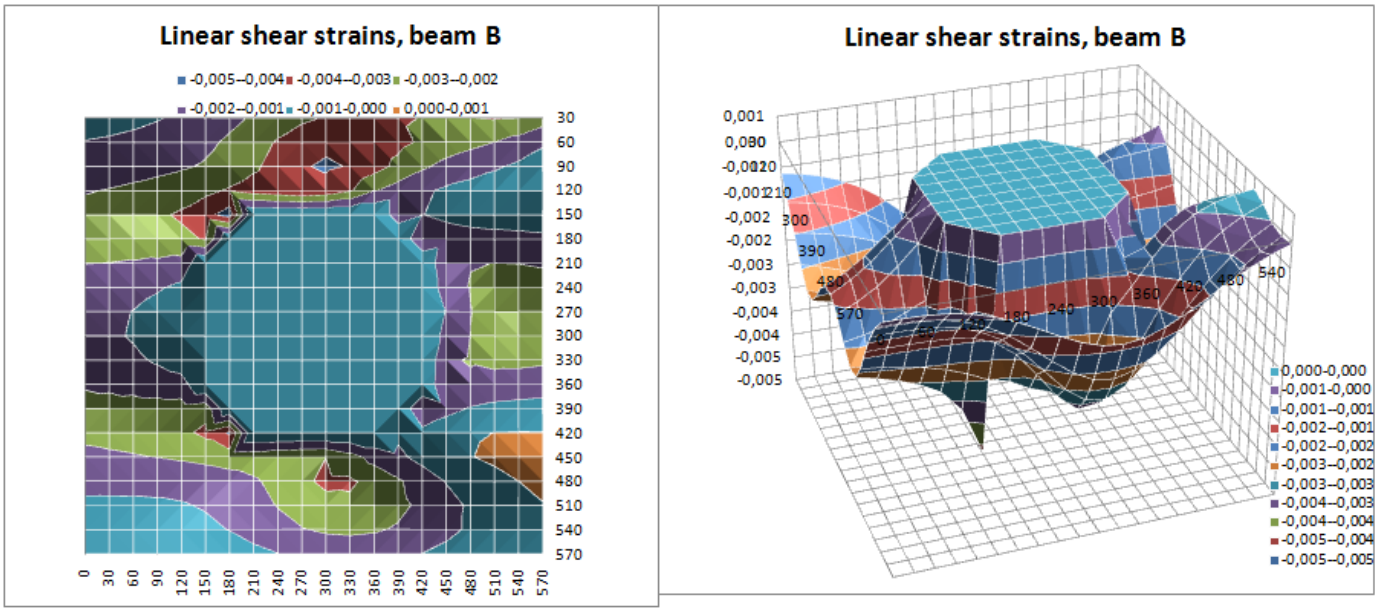

Figure 19: shear strains in the vicinity of the hole at load 29 190N

The shear strain output results are distributed very differently on the two beam types, see Figure 18 and 19. Beam type A has high concentrations of shear above and below the hole, and parable shaped distribution of shear in the mid section of the beam, to the left and the right side of the grid. The peaks arise above and below the hole in the same way, viewing the sections as individual beams that need to transfer twice the shear force each [3].

$$V_{max} = \frac{3}{2} \quad \frac{\frac{1}{2} V}{\frac{1}{4} A} = \quad 3 \, \frac{V}{A} \qquad [3]$$

The parable shaped shear distribution in beam B is of higher value than in beam A. The hole causes principal stresses to act at an angle to the grain in the regions of high stress concentrations, see Figure 1 (Johannesson 1983; Aicher and Höfflin 2000). This results in additional transversal and shear stress and thus strain. In beam B, where the hole is located near the bending moment maximum, the principal stresses will according to theory, be larger resulting in larger additional y- directional and shear stress and strain. It is unclear why the numerical analysis gives higher shear values in beam B as it does not seem to consider the effect of bending moment (see linear strains in Y direction).

3.2.2. Non linear analysis

3.2.2.1. Vertical strains

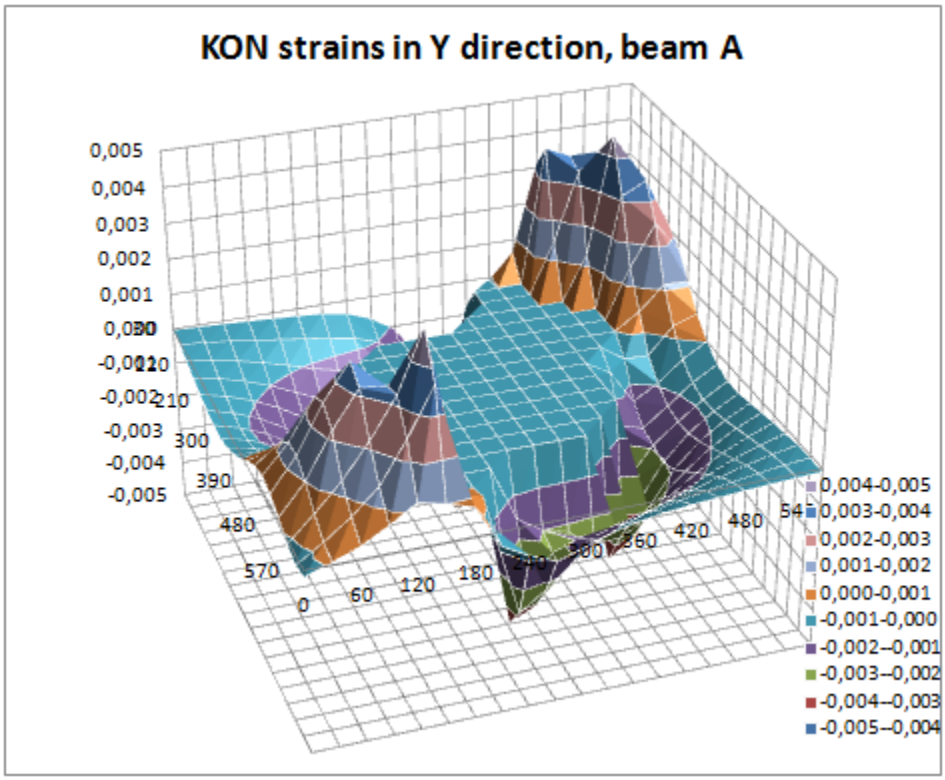

Figure 20: Normal trains in the vicinity of the hole of beam A at load 28 750N

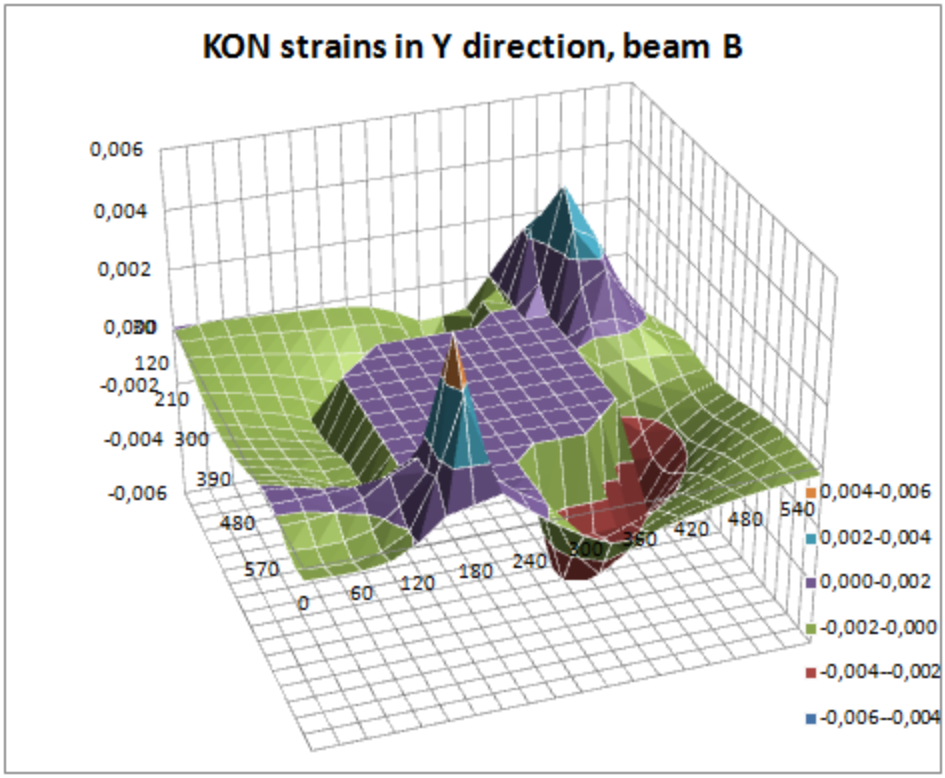

Figure 21: Normal strains in the vicinity of the hole of beam B at load 29 190N

The axial strain results from the KON analysis presented in Figure 20 and 21 for beam A and B respectively, are of significantly higher magnitude than the linear strain results for the same load. The strain peaks in the KON analysis are vicinal to the nodes that have exceeded the criterion [2] discussed in Numerical models of experiments, and which represents a crack. Comparing Figure 20 and Figure 21, there is an obvious difference in magnitude of the strain “mountains” in zone 2 and zone 4. The transversal strain peaks in beam A acts in a larger area than the narrow peaks in beam B. The reason for such narrow peaks in beam B can be the superposed transversal compression from the load cell discussed earlier. The maximum peak in beam B is located in zone 4, and has a value higher than the maximum strain value in beam A. In beam B, the strain peak in zone 2 is located closer the upper beam edge than in the linear analysis.

3.2.2.2 Shear strains

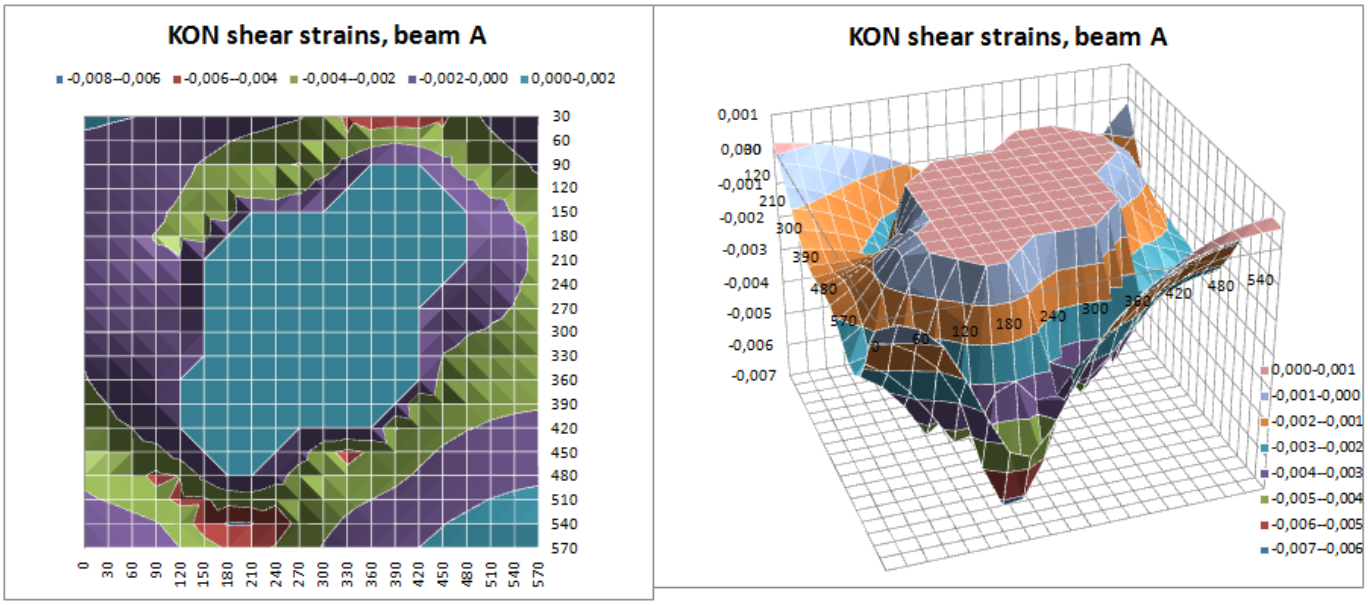

Figure 4: shear strains in the vicinity of the hole at load 28 750N

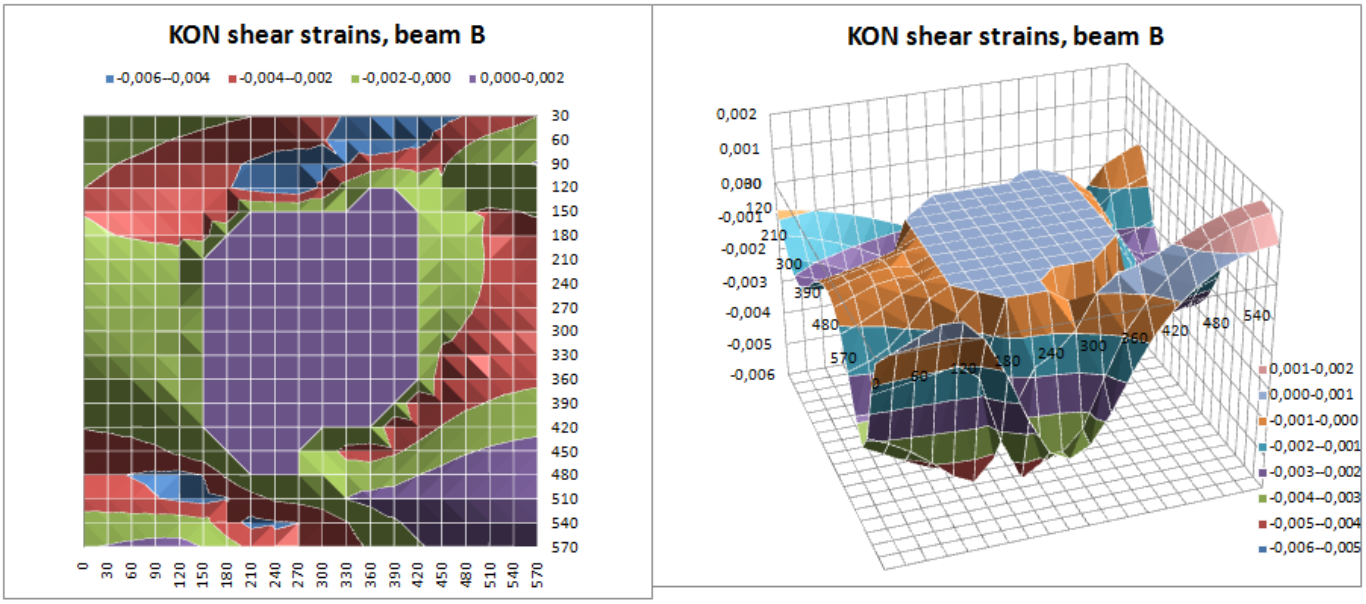

Figure 5: shear strains in the vicinity of the hole at load 29 190N

The maximum shear strain values are for both beam types about twice the size of the shear strains from the linear analysis, see Figure 22 and 23. The distribution of the shear strains is similar to the linear analysis, but it has shifted due to the crack simulation.

The mid sections are in both beams little affected by the crack simulation. The shear strain values in these areas are of the same magnitude as the corresponding areas in linear analysis

There are generally higher shear strains in beam A than beam B.

3.3. Test results

3.3.1. Contour model presentation of measurements

Due to difficulties related to the post processing of photogrammetric results, there is only strain data for beam 2A, 5A, 2B, 3B, 4B and 5B. As the focus of the study is comparing strains on A and B beams, the comparison basis is limited by the amount of A beams, thus strain results from 2A, 2B, 5A and 5B will be presented and discussed.

The contour models presented represent the strain in each dot measured for the load registered in the upper part of the linear elastic range.

Contour models for strain in longitudinal directions are not included. It was a clear tendency of tensile strains in the lower part of the grid, and compressive strains in the upper part of the grid. Higher longitudinal strains were observed for beam type B as anticipated due to higher bending moment.

The measured basic density for the tested beams is presented in Table 3.

Table 3: Average density measured for every lamella in every beam

Beam	Basis density (kg/m^3)
2A	428,8
2B	419,1
5A	404,7
5B	406,1

3.3.1.1. Beam 2A

Figure 24: The back side of the beam. The knot is located in zone 3 in the grid

Figure 25: Beam 2A at failure

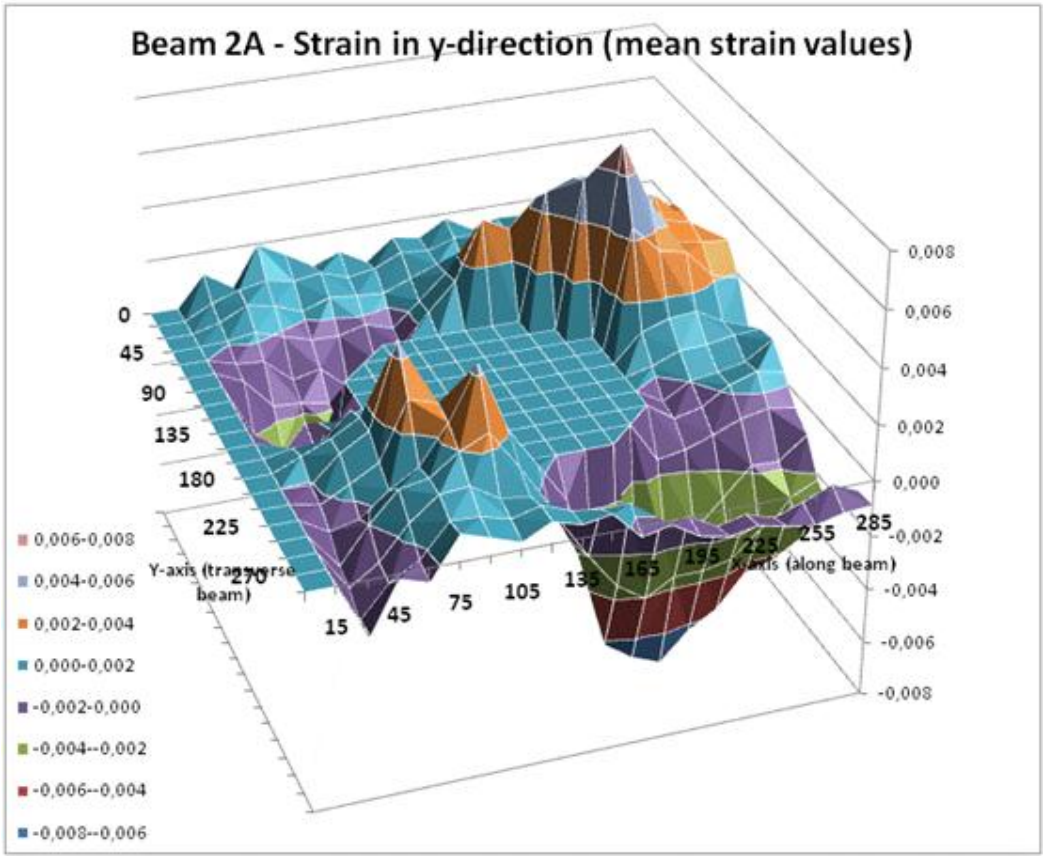

Figure 26: Normal strains perpendicular to grain (mm) at load 28 500N

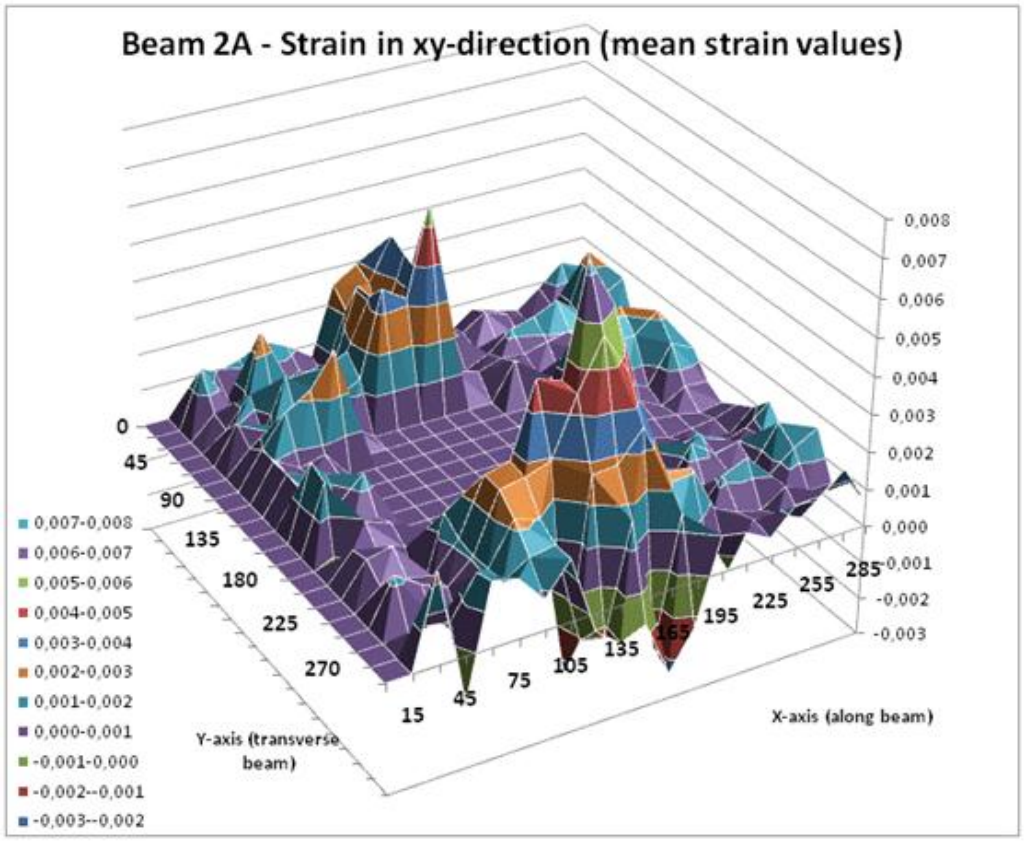

Figure 27: Shear strains (mm) at load 28 500N

3.3.1.2. Beam 2B

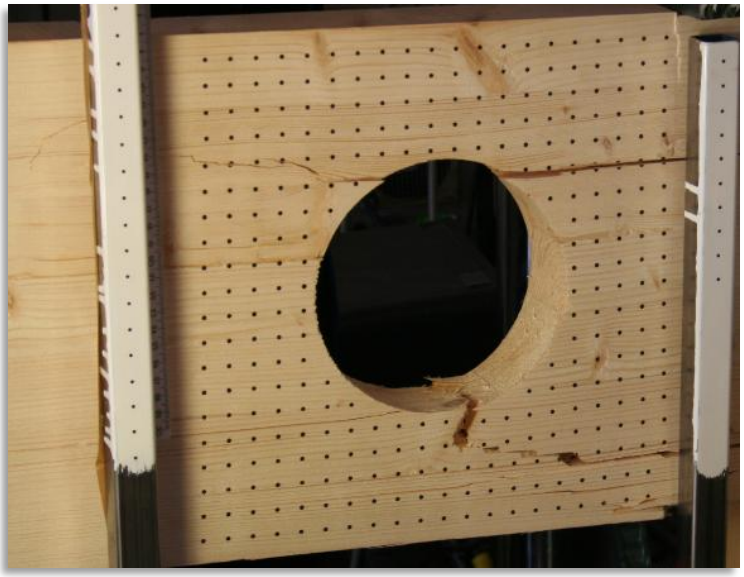

Figure 28: The grid in beam 2B at failure

Figure 29: Knot in zone 2 and 3 on the back side of the beam

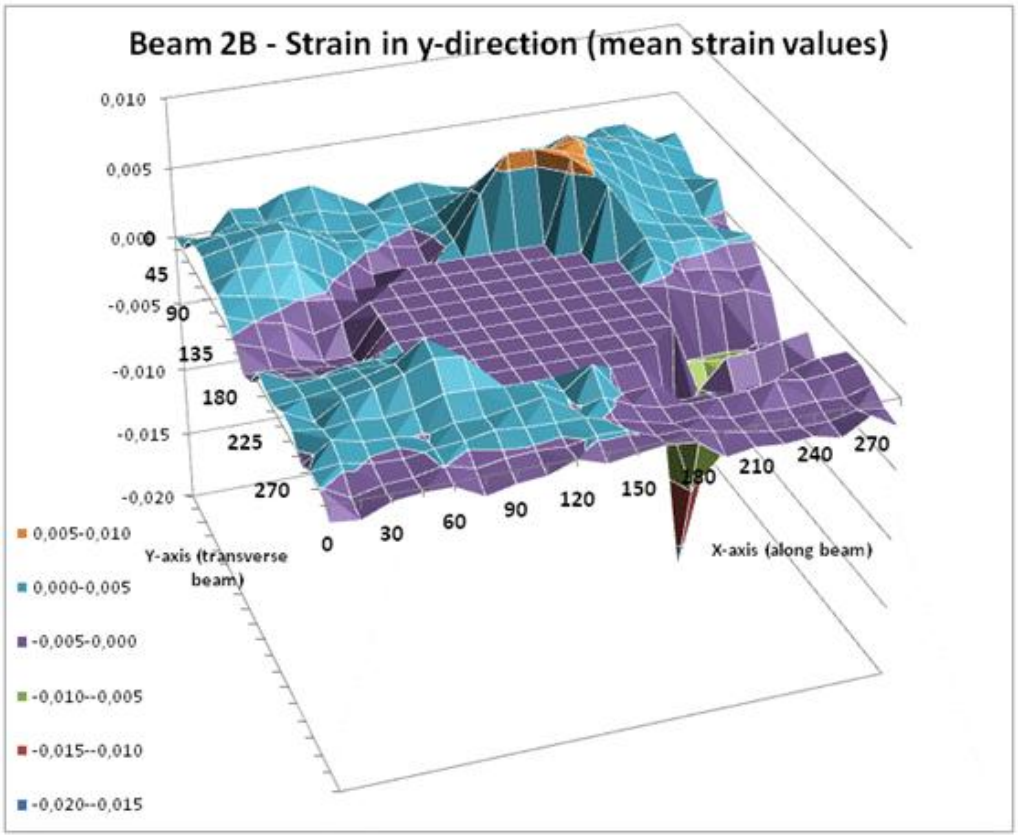

Figure 30: Normal strains perpendicular to grain (mm) at load 31 042N

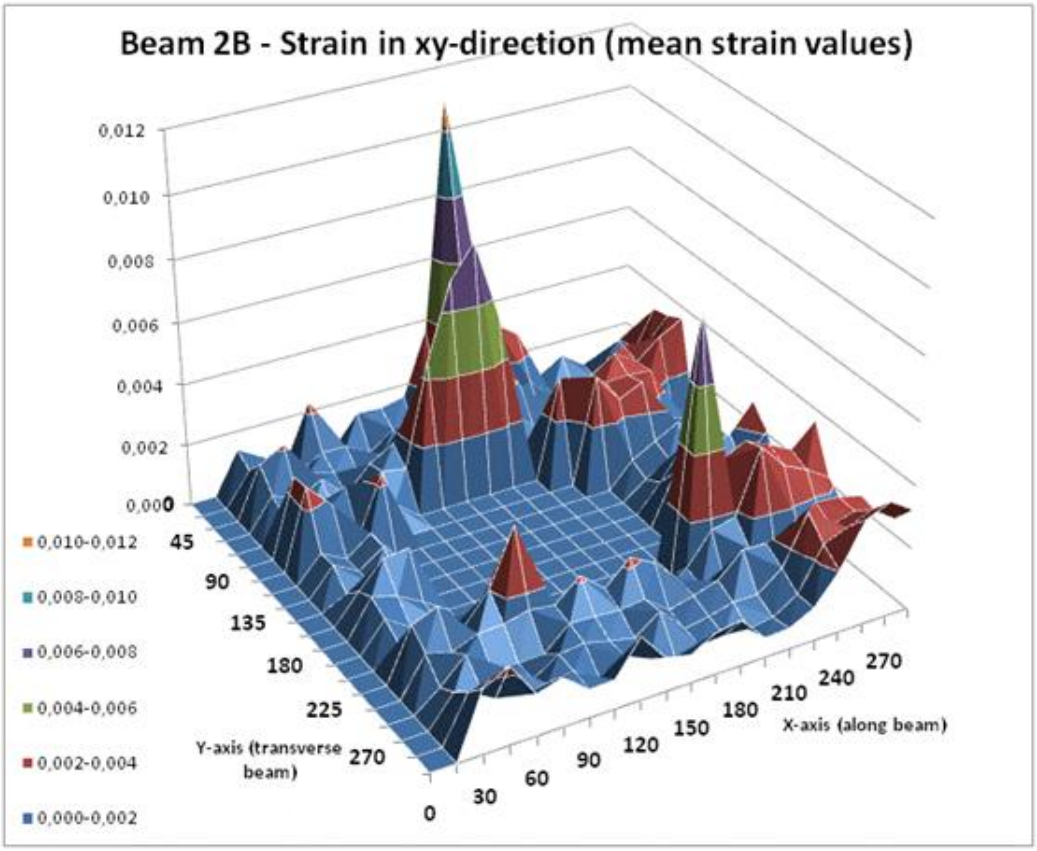

Figure 31: Shear strains (mm) at load 31 042N

3.3.1.3. Beam 5A

Figure 32: The backside of the beam. The knot to the right is located in zone 3

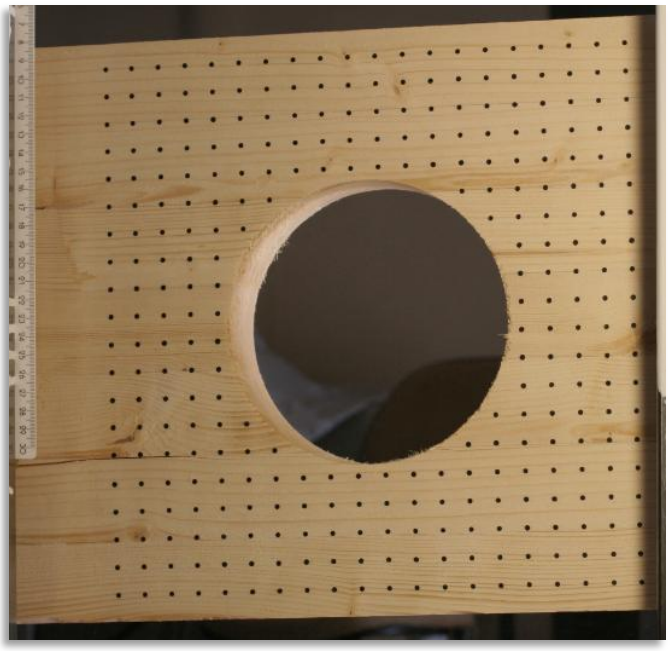

Figure 33: Failure of beam 5A did not occur in the hole vicinity, but due to tension in the lower part of the beam

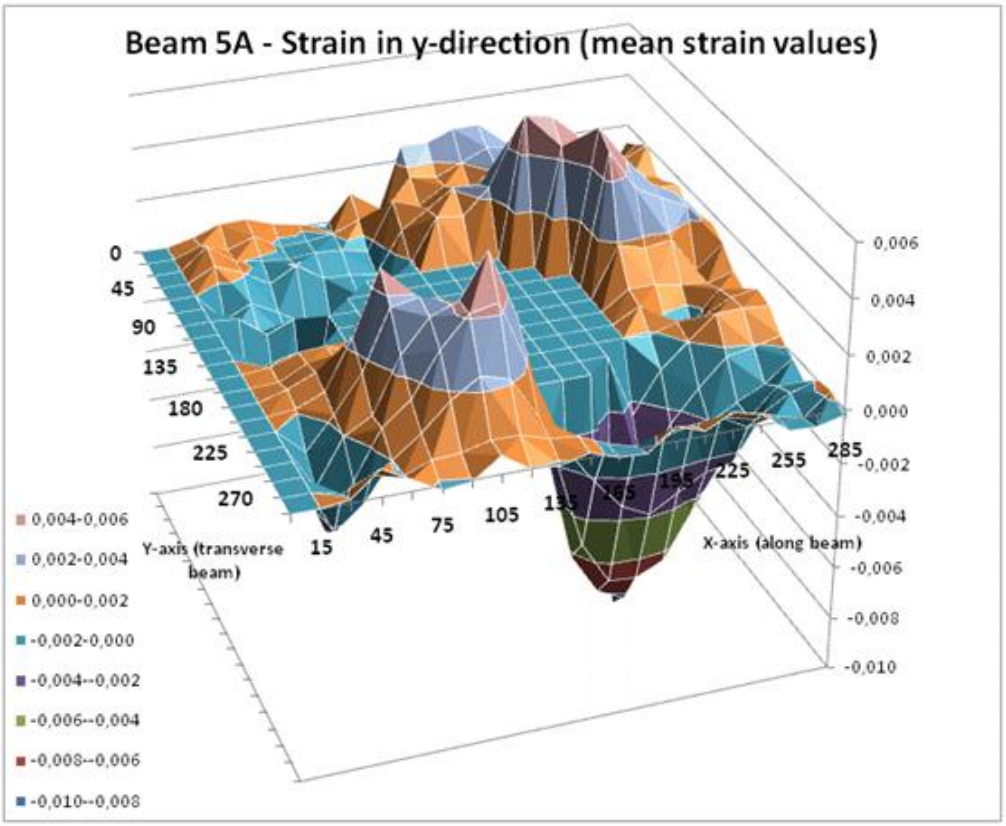

Figure 34: Normal strains perpendicular to grain (mm) at load 35 444N

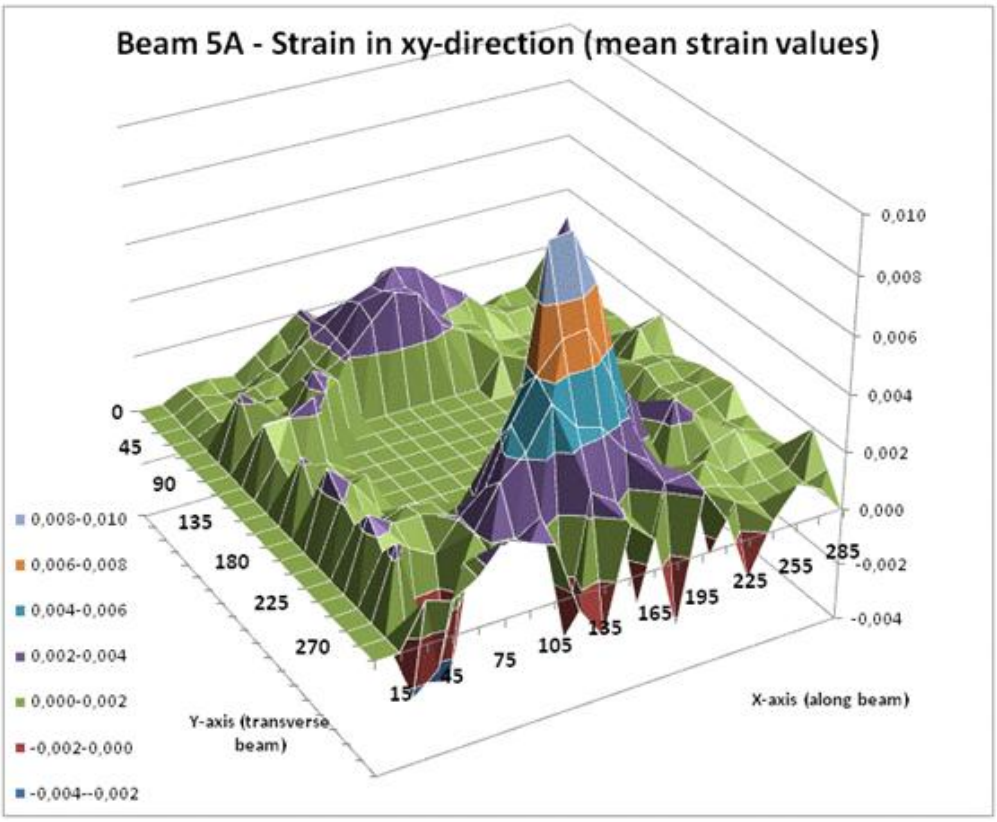

Figure 35: Shear strains (mm) at load 35 444N

3.3.1.4. Beam 5B

Figure 36: The measured grid at failure

Figure 37: The back side of beam 5B. The knot to the right is located in zone 4

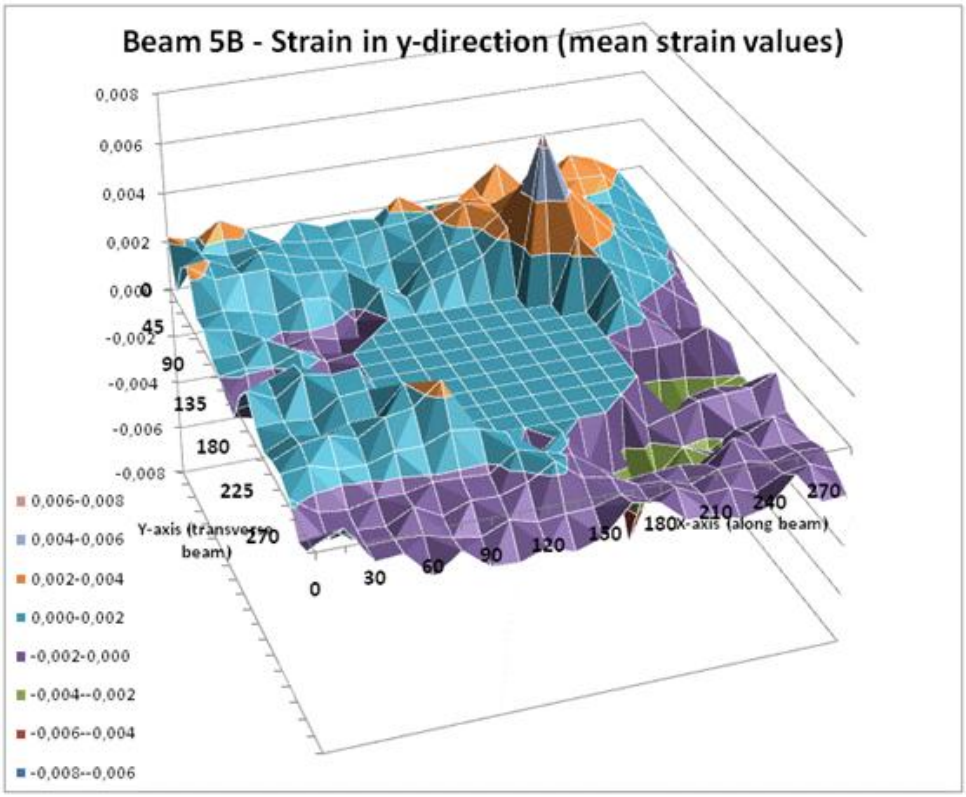

Figure 38: Normal strains perpendicular to grain (mm) at load 24 398N

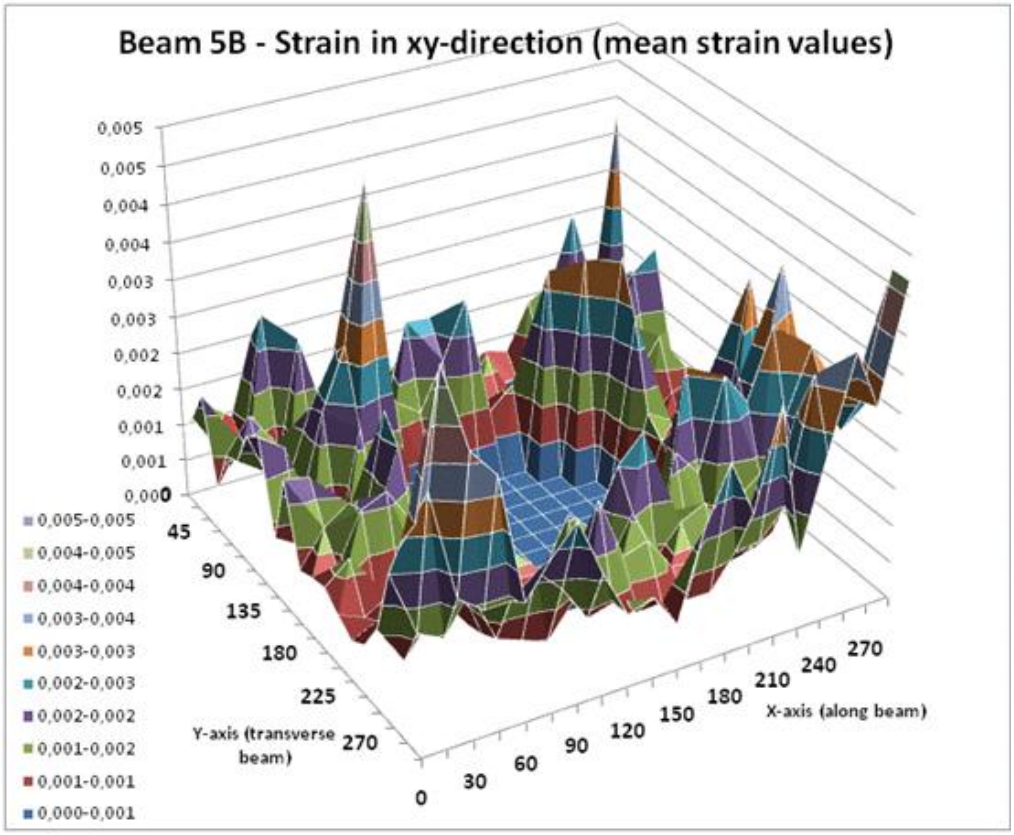

Figure 39: Shear strains (mm) at load 24 398N

3.3.2 Evaluation of contour models of tests

The tendencies shown in the contour plots give an indication of higher y- directional strain values for beam type B.

The maximum shear strain values are higher in beam 2B than in beam 2A, but lower in beam 5A than in beam 5B.

The contour plots of measured strain values show a distribution of axial strains that are in line with earlier theoretical and empirical work (Johannesson 1983; Aicher and Höfflin 2000) The perpendicular to grain tensile strain concentrations are in zone 2 and 4, and the perpendicular to grain compressive strains are concentrated in zone 1 and 3. This distribution is the same for beam 3B and beam 4B, not represented above.

The shear strain distribution seem to have maximum values below the hole for beam 2A and 5A, but a tendency for shear strains for beam type B is difficult to detect in the plots.

3.3.3. Statistical evaluation of measured strains

The average vertical and shear strain of three dots close to the hole in zone 2 see Figure 40, i.e. the most critical zone in terms of perpendicular to grain tension (Aicher and Höfflin 2000), were calculated, and further used in statistical comparison of beam type A and beam type B. Statistical analyses based on actual mean strain values for the selected dots and corresponding load was done for the linear elastic range.

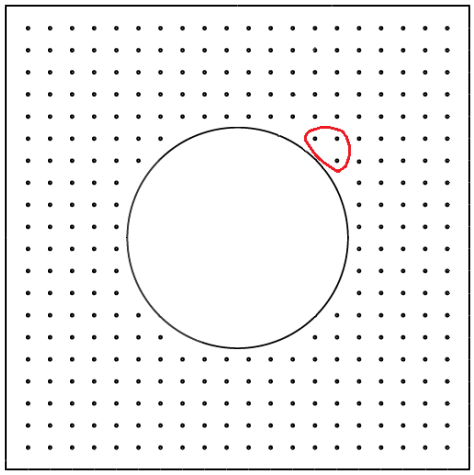

Figure 40: The location of the three dots that were further evaluated

Covariance analysis with load as covariate and beam type as categorical variable and the interaction between the two were performed for the mean values of the selected dots.

3.3.3.1. Strains perpendicular to grain

The results from the covariance analyses estimating normal strain perpendicular to grain (DF: 3, 119, F: 1620.18, P- VALUE < 0.0001, r SQUARE: 0.976) are plot in Figure 41.

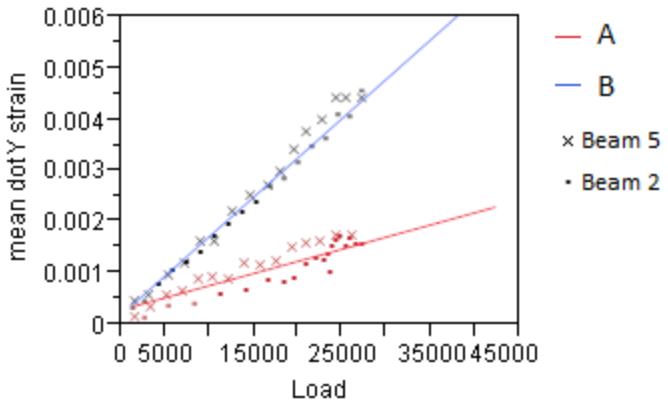

Figure 41: The result of the covariance analysis of perpendicular to grain strains

All three variables (Load, Beam type and Load times Beam type) reduced the residual variance significantly.

Including beam 3B and 4B in the covariate analyses resulted in a lower R square value (0,956) due to more scatter in strain values, see Figure 42, but still the reduction in residual variance was highly significant (DF: 3,100, F: 746.49, P-value < 0.0001).

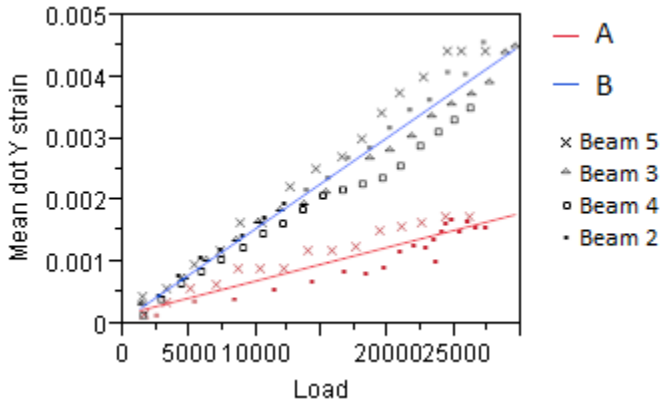

Figure 42: The covariance analysis of normal strains perpendicular to grain including all beams is measured

The significant difference for the normal strains perpendicular to grain in zone 2 between beam type A and beam type B verify earlier research (Aicher and Höfflin 2000) indicating critical effect on the vicinity of a hole when the hole is positioned in a bending moment governed area.

It needs to be emphasized that the statistical tests are only performed for three dots in the critical area of zone 2 in the vicinity of the hole, and do not say anything about the difference in strain elsewhere in the grid. Information about the strains propagating in other parts of the grid is to a certain degree provided by the contour plots.

It is also necessary to emphasize that the statistical significance are based on measurements of very few replicates.

The picture resolution of 8,2 MP which was used in this study would not have given such high F- values and small RMSE values if not mean values from many pictures had been used. Using the mean values from 20 pictures provide a more distinct account of the center of the dots in the grid, practically resulting in a higher picture resolution.

3.3.3.2. Shear strains

The same statistical analyses were done for shear strains, see Figure 43. There were not found significant difference for shear strain values in zone 2 between beam A and beam B. Beam type did not reduce the residual variance significantly (P- value = 0.21). The interaction between beam type and load did not reduce the residual variance either (P- value = 0.99). The shear strains in zone 2 increased linearly with increasing load in the linear elastic range for both beam types.

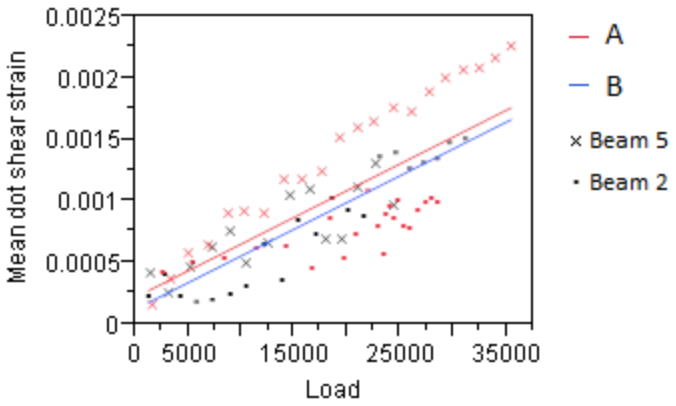

Figure 43: The result of the covariance analysis of shear strains.

The shear strain values were statistically tested including beam 3B and 4B. Neither beam type (P- value = 0.30) nor the interaction between beam type and load (P- value = 0.88) reduced the residual variance significantly. The regression line is shown in Figure 44.

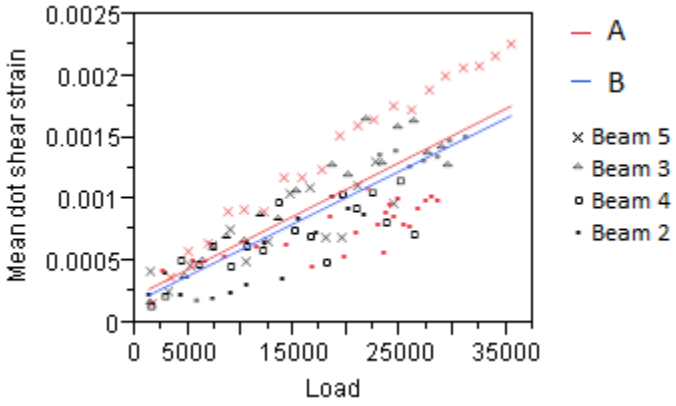

Figure 44: The covariance analysis of normal strains perpendicular to grain including beam 3B and 4B

The tested beams were subjected to three points loading giving even shear distribution in the entire beam. Shear induced by change of principal stress direction due to the hole will however be of higher magnitude in areas with high bending moment. This cannot be shown in the statistical analysis of the difference in shear strains in zone 2 between beam type A and beam type B.

3.4. Evaluation of linear and non linear numerical analysis against test results

Comparing the contour plots of numerical strain values and strains measured from experimental tests, gives a clear indication that the linear FEM analysis done, fit poorly with the strains measured. The normal strains in the y- direction are predicted to be higher in beam type A than in beam type B, the opposite of the measured results.

Initiation of cracks increases the strain values of the surrounding material significantly, clearly indicated by the numerical analysis with KON.

The numerical analysis with the KON method gives a somewhat more realistic picture. It gives a good indication of where the cracks appear. Figure 45 and 47 shows the numerical models of beam A and B, by a load corresponding to the failure load of the beams in Figure 46 and 48.

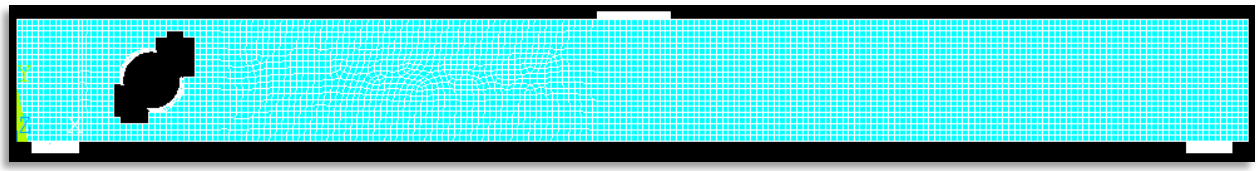

Figure 45: Beam type A, with load 38727N. Black area outside the hole shows the area with killes nodes

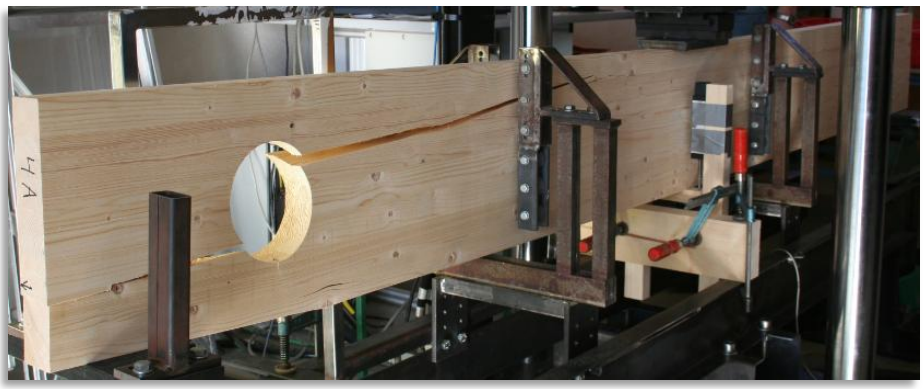

Figure 466: Beam 4A, failure load at 38727 N

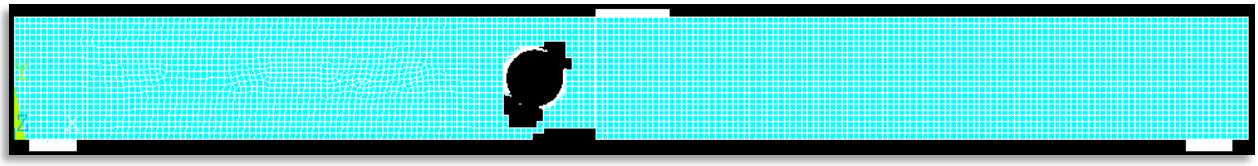

Figure 47: Beam type B, with load 34820N

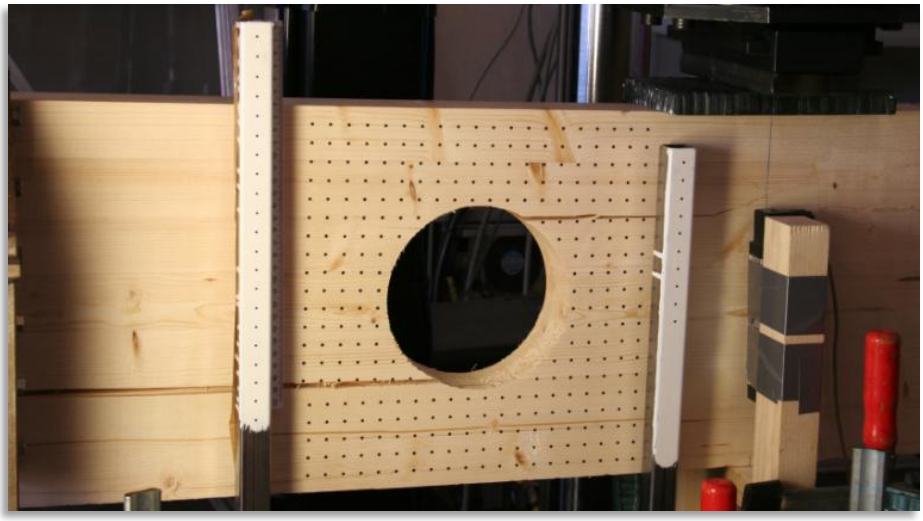

Figure 48: Beam 3B, failure load at 34820 N

When running the analysis with KON, it was possible to observe at what stresses nodes lost their connection, giving a clear indication that normal tension in the y- direction is the critical stress. This is in line with the research of Höfflin and Aicher (2003) "Regarding the magnitude of the three stresses relative to their respective strength values, for instance via a Norris stress interaction criteria, we see that tension stress perpendicular to grain is by far most damage relevant."

Visible cracks were initiated by a load of around 40kN in beam type A, and around 34kN for beam type B (the average value for beam 2A and 5A, and beam 2B, 3B, 4B and 5B respectively). KON is activated by around 9kN for beam type A and around 10kN for beam type B. This is very early compared to when cracks were visible in the test beams.

An explanation of why KON is activated at such low loads is partly that the material parameter input values for the transverse direction are mean values of properties in the tangential and radial plane as transverse isotropic material was assumed. The tangential properties are lower than the radial properties for Norway Spruce (Kollman and Cote 1968; Dahl 2009). The transversal material properties that are used in the numerical analysis are thus lower than the radial properties that are the governing transversal direction in the measured grid on the test beams, see Figure 9. Using the radial direction properties would increase the E modulus by 40 %, and the Poisson's constant by 20%.

The normal strain perpendicular to grain value predictions from the numerical analysis with KON are generally of lower value than the strain measurements from the tests. Similar to the linear FEM analysis, the FEM analysis with KON gives higher strain values in the vertical direction in beam type A than in beam type B. Better knowledge of the stress and strain calculations behind the output results from the numerical analyses is necessary in order to improve the model.

4. Concluding remarks

Photogrammetric strain measurements in the vicinity of a hole in glulam beams have not been reported in the literature so far. Using photogrammetry to measure strains seems to provide good information about strain values on the surface of glued laminated wood in the vicinity of the hole.

It was measured a significant effect of bending moment on the normal strains perpendicular to grain plane in the critical area in the vicinity of the holes. As strain and stress are closely related, these results verify results from earlier empirical stress studies (Kolb and Frech 1977; Penttala 1980; Johannesson 1983), and numerical stress results found by Aicher and Höfflin (2000).

As the normal strains perpendicular to grain were measured to be approximately twice the size in corresponding areas subjected to high bending moment and subjected to low bending moment, it is reason to believe that passive normal strains perpendicular to grain due to compression in the upper part of the beam, are contributing to the severe concentration of normal strains perpendicular to grain in zone 2.

There were not found any significant differences in shear strains in the vicinity of the hole for beams subjected to high bending moment to shear force ratios compared to beams with low bending moment to shear force ratios. It is the shear force resulting from the normal stress disturbance introduced by the hole that expects to cause higher shear strains in zone 2 in the vicinity of the hole. In order to achieve significant differences on the bending moment affect on shear strains, more replicates are needed.

The linear finite element model developed did not give realistic strain values in the vicinity of the hole. Further, the linear analysis did not consider the effect of bending moment on the normal strains in the hole vicinity correctly. The linear analysis did give good indications about the locations of the different strain peaks.

The finite element model considering the propagation of cracks gave strain values closer to the strain values measured on the tested beams, but the analysis still underestimated the strains. The numerical

results also gave higher normal values for beam type A than beam type B, which was the opposite of what the measurements showed.

The results from the numerical analysis with KON points in the direction of the need for a failure mechanic approach to the issue of designing glulam beams with holes. This confirms the conclusions drawn by Scheer and Haase (2000[2]), Stefansson (2001) and Danielsson and Gustafsson (2010).

5. References

1995-1-1, E. (2004). "Eurocode 5: Design of timber structures – Part 1-1:

General - common rules and rules for buildings.".

Aicher, S. and L. Höfflin (2000). "A contribution to the analysis of glulam beams with round holes." Otto-Graf-Journal **11**: 167-180.

Aicher, S. and L. Höfflin (2004). New Design Model for Round Holes in Glulam Beams, MPA, University of Stuttgart

Stuttgart, Germany.

Aicher, S. and L. Höfflin (2006). Load capacity and design of glulam beams with round holes - Safety relevant modifications of design methods according to Eurocode 5 and DIN 1052, MPA Otto-Graf-Institute, University of Stuttgart.

Aicher, S. and L. Höfflin (2008). Fracture behaviour and design of glulam beams with round holes, MPA University Stuttgart.

ANSYS[1] ANSYS® Mechanical, release 13.0, ANSYS Inc.

ANSYS[2] ANSYS®Mechanical, Release 13.0, Help System, Element Reference - Part 1, Element Library, PLANE 42, ANSYS, Inc.

Bodig, J. and B. A. Jayne (1982). Mechanics of Wood and Wood Composites, Krieger Pub Co.

Choi, D., J. L. Thorpe, et al. (1991). "Image analysis to measure strain in wood and paper." Wood Science and Technology **25**: 251-262.

Dahl, K. B. (2009). Mechanical properties of clear wood from Norway spruce. Departement of Structuarl Engineering. Trondheim, NTNU. **Doctoral thesis**.

Danielsson, H. (2009). The strength of glulam beams with holes, A Survey of Tests and Calculation Methods. Departement of Construction Sciences. Lund, University of Lund. **Post Graduate**.

Danielsson, H. and P. J. Gustafsson (2010). "A probabilistic fracture mechanics method and strength analysis of glulam beams with holes." European Journal of Wood and Wood Products.

Franke, S., B. Franke, et al. (2007). "Strain analysis of wood components by close range photogrammetry." Materials and Structures **40**: 37–46.

Gustafsson, P. J. (2003). "Fracture perpendicular to grain - structural applications." **Timber Engineering**.

Gustafsson, P. J. and B. Enquist (1988). Träbalks hållfasthet vid rätvinklig urtagning, Division of Structural Mechanics, Lund University.

Höfflin, L. (2005). Runde Durchbrüche in Brettschichtholzträger - Experimentelle und theoretische Untersuchungen. MPA Otto-Graf-Institute, University of Stuttgart. **Dissertation**.

Höfflin, L. and S. Aicher (2003). "Design of rectangular holes in glulam beams." Otto-Graf-Journal **14**: 211 - 229.

Johannesson, B. (1977). Holes in plywood beams and glued laminated timber beams, Stress concentrations and crack loads. Göteborg.

Johannesson, B. (1983). Design problems for glulam beams with holes. Göteborg.

Kolb, H. and P. Frech (1977). "Untersuchungen an durchbrochenen Bindern aus Brettschichtholz." Holz als Roh - und Werkstoff **35**: 125-134.

Kollman, F. F. P. and W. A. J. Cote (1968). Principles of Wood Science and Technology. Berlin and New York, Springer-Verlag.

Norris, C. B. (1962). Strength of orthotropic materials subjected to combined stresses. Madison, Wisconsin, Forest Products Laboratory

United States Department of Agriculture Forest Service

University of Wisconsin.

NS (1999). Norsk Standard: Prosjektering av trekonstruksjoner, Beregnings- og konstruksjonsregler, Del 1: Almnne regler.

Penttala, V. (1980). Reiallinen liimapuupalkki. Division of Structural Engineering. Otaniemi, Helsinki University of Technology.

Riipola, K. (1995). "Timber beams with holes: Fracture mechanics approach." Journal of Structural Engineering, **121**(2): 225-239.

SAS (statistical discovery). Inc., Cary, N. C., USA.

Scheer, C. and K. Haase (2000[1]). "Holes in glulam beams, Part 1: Theoretical stress analyses." Holz als Roh - und Werkstoff **58**: 153-161.

Scheer, C. and K. Haase (2000[2]). "Holes in glulam beams, Part 2: Fracture mechanics analyses." Holz als Roh - und Werkstoff **58**: 217-228.

Stefansson, F. (2001). Fracture analysis of orthotropic beams - Linear elastic and nonlinear methods. Licentiate Dissertation. Lund, Division of Structural Mechanics. **Report TVSM-3029**.

Tordivel Scorpion.